

Long-lived quantum coherences in a V-type system strongly driven by a thermal environment

Suyesh Koyu and Timur V. Tscherbul*

Department of Physics, University of Nevada, Reno, Nevada 89557, USA (Received 1 December 2017; revised manuscript received 27 May 2018; published 7 August 2018)

We explore the coherent dynamics of a three-level V-type system interacting with a thermal bath in the regime where thermal excitation occurs much faster than spontaneous decay. We present analytic solutions of the Bloch-Redfield quantum master equations, which show that strong incoherent pumping can generate long-lived quantum coherences among the excited states of the V-type system in the overdamped regime defined by the condition $\Delta/(\bar{n}\gamma) < f(p)$, where Δ is the excited-state level splitting, γ is the spontaneous decay rate, $\bar{n} \gg 1$ is the effective photon occupation number proportional to the pumping intensity, and $f(p)$ is a universal function of the transition dipole alignment parameter p . In the limit of nearly parallel transition dipoles ($p \rightarrow 1$) the coherence lifetime $\tau_c = 1.34(\bar{n}/\gamma)(\Delta/\gamma)^{-2}$ scales linearly with \bar{n} and is enhanced by the factor $0.67\bar{n}$ with respect to the weak-pumping limit [Phys. Rev. Lett. **113**, 113601 (2014); J. Chem. Phys. **144**, 244108 (2016)]. We also establish the existence of long-lived quasistationary states, which occur in the overdamped regime and affect the process of thermalization of the V-type system with the bath, slowing down the approach to thermal equilibrium. In the case of nonparallel transition dipole moments ($p < 1$), no quasistationary states are formed and the coherence lifetime decreases sharply. The sharp transition between the different regimes of coherent dynamics is due to an interplay between coherence-generating Fano interference and various coherence-destroying processes (such as stimulated decay). Using a newly developed effective decoherence rate model, we find that in the limit $p \rightarrow 1$ the rates of coherence generation and decay are almost exactly balanced and the effective decoherence rate is minimized, leading to long coherence lifetimes. Our results reveal new regimes of long-lived quantum coherent dynamics, which could be observed in thermally driven atomic and molecular systems.

DOI: [10.1103/PhysRevA.98.023811](https://doi.org/10.1103/PhysRevA.98.023811)**I. INTRODUCTION**

Relaxation and loss of coherence in multilevel quantum systems caused by their interaction with a thermal environment is a subject of paramount importance in many areas of physics including quantum optics [1–3], quantum sensing [4], and quantum information processing [5]. While interaction with the environment is generally believed to destroy any quantum coherence initially present in the system [1], recent theoretical studies have challenged this point of view suggesting a number of mechanisms for the generation of quantum (Fano) coherences in multilevel systems driven by thermal noise [6–16]. These mechanisms have attracted attention due to their predicted ability to enhance the efficiency of quantum heat engines [11,12] and as potential sources of nontrivial quantum effects in photosynthetic light harvesting [13–15].

The noise-induced Fano coherences can be understood as arising from quantum interference of the different incoherent excitation pathways originating from the same initial state [6,9]. The mathematical description of the interference effects requires the use of nonsecular Bloch-Redfield (BR) theory, in which populations and coherences are treated on the same footing, leading to more complex dynamics than predicted by the secular rate equations [13,14,17]. Such noise-induced coherent dynamics are responsible for a number of remarkable effects such as vacuum-induced coherence [18], enhanced

efficiency of quantum heat engines [11,12], and long-lived quasistationary states [13]. Note that the secular approximation cannot be justified in systems with nearly degenerate energy levels, where the system evolution time can be much longer than the timescale of interest [13].

The three-level V-type system comprising a single ground state coupled by the system-bath interaction to a pair of excited states (see Fig. 1) serves as a minimal model of a multilevel quantum system exhibiting nontrivial Fano coherence dynamics. This system has been extensively studied in the weak-pumping limit (relevant for photosynthetic light harvesting) where incoherent excitation occurs much more slowly than spontaneous emission. In this limit, the coherent dynamics of the V-type system is determined by the ratio $\zeta = \frac{1}{2}(\gamma_a + \gamma_b)/\Delta_p$, where $\Delta_p = \sqrt{\Delta^2 + (1 - p^2)\gamma_a\gamma_b}$ is the renormalized excited-level splitting, γ_a and γ_b are the spontaneous decay rates, and p is the angle between the transition dipole moments of the $c \rightarrow a$ and $c \rightarrow b$ transitions (see Fig. 1) [14]. The two-photon coherences between the excited states of the V-type system exhibit damped oscillations in the regime where the excited levels are widely spaced ($\zeta \ll 1$). In the opposite regime of small level spacing ($\zeta \gg 1$), the coherences evolve monotonously and can survive for an arbitrarily long time $\tau_c = 2\sqrt{\gamma_a\gamma_b}/\Delta_p^2$ [13,14].

While the weak pumping regime of noise-induced coherent dynamics is well understood [9,13–15], much less is known about the opposite limit where incoherent excitation occurs much faster than spontaneous decay. The strong pumping regime is central to the theory of quantum heat engines,

*ttscherbul@unr.edu

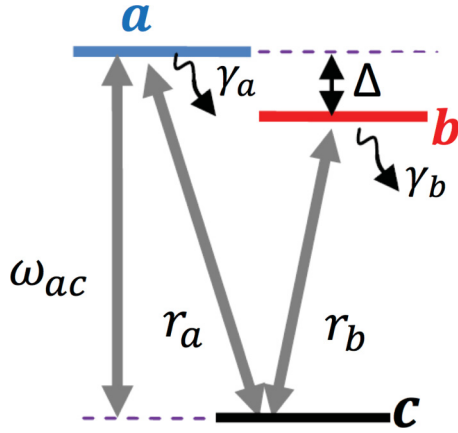


FIG. 1. A schematic depiction of the three-level V-type system characterized by the excited-state energy splitting $\Delta = \omega_{ab}$, the rates of spontaneous decay into the vacuum modes of the bath γ_i ($i = a, b$), and the thermal pumping rates $r_i = \gamma_i \bar{n}$. The factor $p = \vec{\mu}_{ac} \cdot \vec{\mu}_{bc} / |\vec{\mu}_{ac}| |\vec{\mu}_{bc}|$ quantifies the alignment of the transition dipole moment vectors $\vec{\mu}_{ac}$ and $\vec{\mu}_{bc}$.

where quantum coherence has been predicted to enhance the engine's efficiency [11,12]. Accordingly, the generation and steady-state properties of quantum coherences in this regime have been studied in closed-cycle quantum heat engine models [11] and in the degenerate Λ -type system [10]. However, these studies did not explore the time dynamics of the coherences as a function of the system's excited-state splitting and radiative decay rates. In addition, the quantum heat engine studies [11,12] considered a more complex case of a five-level system interacting with two baths, where the coherences emerge as a result of nonequilibrium transport dynamics involving both of the baths. This leaves open the question of whether strong incoherent driving can generate coherences in multilevel quantum systems interacting with a single thermal bath.

Here we address this question by presenting a theoretical analysis of the quantum dynamics of a V-type system strongly driven by a thermal bath. We derive closed-form analytic solutions of the Bloch-Redfield (BR) quantum master equations, which show that (1) quantum coherences can be generated by strong incoherent driving provided that the transition dipole moments of the V-type system are nearly perfectly aligned, (2) the coherence lifetime scales linearly with the pumping intensity \bar{n} and quadratically with the inverse excited-level spacing γ/Δ , and (3) the long-lived coherences occur in conjunction with quasisteady states, in which excited-state populations deviate strongly from those in thermodynamic equilibrium. These results suggest the possibility of observing long-lived coherence dynamics in strongly driven Rydberg atoms and polyatomic molecules. Significantly, we reveal a sharp transition between the long-lived and short-lived coherence regimes, which occurs as the transition dipole alignment parameter p is decreased below a critical value $p_c \simeq 1$. To elucidate the physical origin of our results, we develop an effective decoherence rate model, which accounts for the processes responsible for the formation and decay of Fano coherences, and provides a qualitative explanation of the observed coherent dynamics and its sharp variation with p .

This paper is structured as follows. In Sec. II we present the theoretical formalism based on the BR master equations and outline the procedure of their analytical solution. The dynamical regimes of the strongly driven V-type system are classified in Sec. II B. Section II C presents our analytical results for noise-induced coherence lifetimes and gives a preliminary discussion of the populations and coherences. Section II D introduces the effective decoherence rate model, which is then used to clarify the physical origin of the different dynamical regimes. Section II E compares the strongly driven and weakly driven regimes of noise-induced coherent dynamics. Section IV summarizes the main findings of this work and outlines an experimental scenario for observing the noise-induced coherences.

II. THEORY

A. Bloch-Redfield equations and their general solution

Consider a three-level V-type system weakly coupled to a thermal environment (see Fig. 1). The system resides in the ground state $|c\rangle$ [i.e., $\rho_{cc}(0) = 1$] before the system-environment coupling is suddenly turned on at $t = 0$, leading to the population transfer to the excited states $|a\rangle$ and $|b\rangle$. To describe the time evolution of the system, we use a quantum master equation approach based on the Liouville-von Neumann equation for the density operator of the system+bath tracing over the bath modes, and adopting the Markov approximation for bath correlation functions, we arrive at the Bloch-Redfield (BR) master equation for the reduced density matrix of the V-type system [8,9,13,14]

$$\begin{aligned} \dot{\rho}_{ii} &= -(r_i + \gamma_i)\rho_{ii} + r_i\rho_{cc} - p(\sqrt{r_a r_b} + \sqrt{\gamma_a \gamma_b})\rho_{ab}^R, \quad (1) \\ \dot{\rho}_{ab} &= -\frac{1}{2}(r_a + r_b + \gamma_a + \gamma_b)\rho_{ab} - i\rho_{ab}\Delta \\ &\quad + \frac{p}{2}\sqrt{r_a r_b}(2\rho_{cc} - \rho_{aa} - \rho_{bb}) - \frac{p}{2}\sqrt{\gamma_a \gamma_b}(\rho_{aa} + \rho_{bb}), \quad (2) \end{aligned}$$

where a , b , and c are the system's energy eigenstates, the two-photon coherence $\rho_{ab} = \rho_{ab}^R + i\rho_{ab}^I$ is given as a sum of its real and imaginary parts, and we have used the conservation of probability condition to express $\rho_{cc} = 1 - \rho_{aa} - \rho_{bb}$.

The BR equations are parametrized by the excited-state energy splitting $\Delta = \omega_{ab}$ (see Fig. 1), the system-bath coupling parameters γ_i ($i = a, b$) which determine the rate of spontaneous decay into the vacuum modes of the bath, and the (pseudo)thermal pumping rates $r_i = \gamma_i \bar{n}$ [16], where \bar{n} is the effective occupation number of thermal modes at the transition frequency ω_{ac} (see Fig. 1). In thermal equilibrium, $\bar{n} = (e^{\beta\omega_0} - 1)^{-1}$, where $\beta = 1/k_B T$, T is the temperature of the bath, and k_B is Boltzmann's constant. An important parameter $p = \frac{\vec{\mu}_{ac} \cdot \vec{\mu}_{bc}}{|\vec{\mu}_{ac}| |\vec{\mu}_{bc}|}$ quantifies the alignment of the transition dipole moment vectors $\vec{\mu}_{ac}$ and $\vec{\mu}_{bc}$ [8,9,13,14]. We will show that the solutions of the BR equations tend to be extremely sensitive to the value of p . Note that for $p = 0$, the BR equations reduce to the standard Pauli rate equations, which give coherence-free dynamics [8,9,13,14]. We will therefore focus on the nontrivial case of $p \neq 0$.

The BR quantum master equations (1) generally describe the dynamics of the V-type system weakly interacting with stochastic bosonic fields, such as photons or phonons [2]. Here we will consider the BR equations in a quantum optical context, relevant to the incoherent light excitation of quantum heat engines in the strong pumping limit $\bar{n} \gg 1$. We can then identify $\gamma_i = \frac{\omega_{ci}^3 |\mu_{ci}|^2}{3\pi\epsilon_0\hbar c^3}$ with the spontaneous emission rate of the excited level $i = a, b$. Furthermore, $r_i = B_i W(\omega_{ci})$ are the incoherent pumping rates of $|c\rangle \leftrightarrow |i\rangle$ transitions with $B_i = \frac{\pi |\mu_{ci}|^2}{3\epsilon_0\hbar^2}$ being the Einstein's B coefficients and $W(\omega_{ci})$ is the intensity of the incident blackbody radiation at the corresponding transition frequencies. Finally, $r_i = \bar{n}\gamma_i$ are the incoherent absorption rates defined in terms of the effective photon occupation number $\bar{n} = B_i W(\omega_{ci})/\gamma_i$ [9,13,16], which is proportional to the pumping intensity.

A comment is in order regarding the validity of the BR quantum master equations in the strong-pumping limit. The *weak-coupling* assumption underlying the BR equations holds as long as the system-bath coupling (as quantified by the incoherent pumping rates r) is much smaller than the energy gap ω_{ac} between the ground and excited energy eigenstates (see Fig. 1). This condition is well satisfied for typical optical frequencies ($\omega_{ac} \sim 10^6$ GHz [2]) and incoherent pumping rates ($r_i = 1-10^3$ GHz) corresponding to the effective photon occupation numbers $\bar{n} = 10-10^3$ typically used in few-level models of quantum heat engines [11,12,20,21]. Thus, the strong-pumping condition $r \gg \gamma$ is consistent with the weak-coupling limit. In contrast, the Markovian assumption is expected to break down at very large pumping rates approaching the inverse bath correlation times $1/\tau_c$. In this limit, the BR equations remain valid as long as $r_i \ll 1/\tau_c$. For incoherent pumping with solar light ($\tau_c \sim 1.3$ fs), this condition implies $\bar{n} \ll 1/(\tau_c\gamma_i) \simeq 10^6$, which is much larger than the effective photon occupation numbers considered here ($\bar{n} = 10^2-10^3$). Following previous theoretical work [11,12,20,21], we neglect multiphoton transitions originating from the excited states of the V-type system.

Here we consider the case of a symmetric V-type system, where $\gamma_a = \gamma_b = \gamma$, $r_a = r_b = r$, and hence $\rho_{aa}(t) = \rho_{bb}(t)$ [13]. The imposed symmetry simplifies the analytical solution of the BR equations to a great extent, while retaining the essential features of the dynamics [13,14]. The BR master equations for the symmetric V-type system (1) can be expressed in matrix-vector form

$$\dot{\mathbf{x}}(t) = \mathbf{A}\mathbf{x}(t) + \mathbf{d}, \quad (3)$$

where $\mathbf{x}(t) = [\rho_{aa}(t), \rho_{ab}^R(t), \rho_{ab}^I(t)]^T$ is the state vector in the Liouville representation, where the elements of a $N \times N$ density matrix are represented by a vector of dimension N^2 [19], and $\mathbf{d} = [r, pr, 0]^T$ is the driving vector. Note that the state vector excludes the ground-state population and the one-photon coherences ρ_{ac} and ρ_{bc} , which evolve independently [8]. The coefficient matrix \mathbf{A} in Eq. (3) is given by

$$\mathbf{A} = \begin{bmatrix} -(3r + \gamma) & -p(r + \gamma) & 0 \\ -p(3r + \gamma) & -(r + \gamma) & \Delta \\ 0 & -\Delta & -(r + \gamma) \end{bmatrix}. \quad (4)$$

The general solution of the system of inhomogeneous differential equations (3) may be obtained as [22]

$$\mathbf{x}(t) = e^{\mathbf{A}t} \mathbf{x}_0 + \int_0^t ds e^{\mathbf{A}(t-s)} \mathbf{d}(s), \quad (5)$$

where \mathbf{x}_0 specifies the initial conditions for the density matrix, and $\mathbf{d}(s)$ is the driving vector defined above. Since our interest here is in the generation of noise-induced Fano coherences by incoherent driving, we choose a coherence-free initial state $\rho_{cc}(t=0) = 1$, or $\mathbf{x}_0 = (0, 0, 0)^T$, corresponding to the V-type system initially in the ground state. The exponent of matrix \mathbf{A} in Eq. (5) and the density matrix dynamics $\mathbf{x}(t)$ can be evaluated analytically in the limit $\bar{n} \gg 1$ by expanding the matrix elements in the small parameter $x = 1/\bar{n}$ as described in the Appendix.

B. Dynamical regimes

The behavior of the general solution of the BR equations (5) is determined by the eigenvalue spectrum λ_k of the coefficient matrix \mathbf{A} . While the spectrum can be obtained analytically as described below and in the Appendix, its general features can be understood by examining the discriminant D of the characteristic equation for \mathbf{A} ,

$$D = B^3 + [C - \frac{3}{2}A(B + A^2)]^2, \quad (6)$$

where

$$\begin{aligned} A &= \frac{1}{3}(5r + 3\gamma), \\ B &= \frac{1}{3}[\Delta^2 + (r + \gamma)^2 + (2 - p^2)(r + \gamma)(3r + \gamma)] - A^2, \\ C &= \frac{1}{2}(3r + \gamma)[\Delta^2 + (1 - p^2)(r + \gamma)^2] + A^3. \end{aligned} \quad (7)$$

The above expressions are valid for all p .

Depending on the sign of D , three dynamical regimes can be distinguished:

(1) *Underdamped regime* ($D > 0$). If the discriminant (6) is positive, one of the eigenvalues of \mathbf{A} is real and the other two eigenvalues are complex. The corresponding normal modes include an exponentially decaying eigenmode and two oscillating eigenmodes. Using the analogy with the damped harmonic oscillator [14], we will refer to this regime as *underdamped*.

(2) *Overdamped regime* ($D < 0$). If the discriminant (6) is negative, all of the eigenvalues λ_k are real with $\text{Re}(\lambda_k) < 0$, and thus all normal modes decay exponentially. Following our previous work [14], we will refer to this regime as *overdamped*.

(3) *Critical regime* ($D = 0$). If the discriminant (6) vanishes, all of the eigenvalues λ_k are real with at least two of them being equal. This is the *critical regime* [14], which marks a transition between the underdamped and overdamped regimes.

To classify the dynamical regimes of the strongly driven V-type system, we therefore need to identify the regions of the parameter space where the discriminant (6) takes on positive and negative values. As shown in the Appendix, the discriminant can be expressed as a polynomial function of the occupation number $\bar{n} = r/\gamma$,

$$D = \frac{\gamma^6}{108} \sum_{k=0}^6 d_k \bar{n}^k, \quad (8)$$

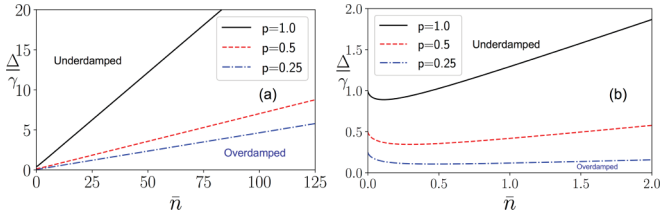


FIG. 2. (a) Lines of zero discriminant separating the overdamped ($D < 0$) from underdamped ($D > 0$) regions for large Δ/γ and \bar{n} . The overdamped behavior occurs in the bottom right corner of the plot, where $\Delta/\gamma \ll \bar{n}$. (b) A zoom into the small (Δ/γ , \bar{n}) region. Regions below the zero- D lines correspond to overdamped dynamics; those above the zero- D lines correspond to underdamped dynamics.

where the coefficients d_k depend on the ratio Δ/γ of the excited-state splitting to the radiative decay rate and the transition dipole alignment factor p .

Figure 2 shows the lines of zero discriminant separating the overdamped ($D < 0$) from underdamped ($D > 0$) regimes as a function of the average photon occupation number \bar{n} and the excited-state energy splitting Δ/γ for selected values of p . A contour plot of the discriminant is shown in Fig. 3. We observe that when both \bar{n} and Δ/γ are large, the solution of the equation $D = 0$ is given by the straight line $\Delta/\gamma = f(p)\bar{n}$. It can be shown analytically (see the Appendix) that the slope of the line $f(p)$ is a function of p only. While an explicit expression for the slope function $f(p)$ can be obtained analytically by solving the equation $D = 0$ [see Eq. (A21) of the Appendix] it is extremely cumbersome. A plot of $f(p)$ presented in Fig. 4(a) shows that the slope function increases monotonically from 0 to 0.6 as p is varied between 0 and 1.

As illustrated in Fig. 3(a), the discriminant is positive in the underdamped region above the zero- D lines, where the coherences exhibit damped oscillations. Below the $D = 0$ lines, the sign of D changes from positive to negative and the V-type system enters the overdamped regime, with coherences evolving monotonously as a function of time. Since, as shown above, the zero- D lines are described by $\Delta/\gamma = f(p)\bar{n}$ at large \bar{n} and Δ/γ , the dynamical regimes of the strongly driven V-type system can be classified based on a single dimensionless parameter $\Delta/(\bar{n}\gamma) = \Delta/r$. The overdamped regime is defined by the condition $\Delta/(\bar{n}\gamma) < f(p)$, whereas the underdamped regime is defined by $\Delta/(\bar{n}\gamma) > f(p)$. For perfectly aligned transition dipole moments, we have $f(1) = 0.6$ [see Fig. 4(a)]

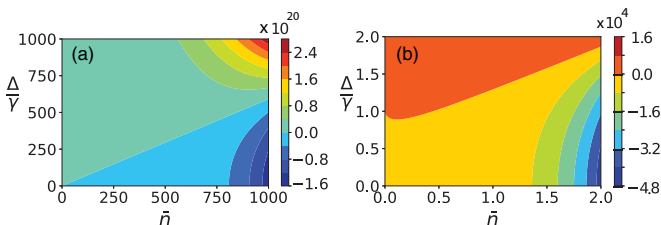


FIG. 3. (a) A contour plot of the discriminant D for large $\frac{\Delta}{\gamma}$ and \bar{n} and $p = 1.0$. (b) A zoom into the region close to the origin ($\frac{\Delta}{\gamma} \ll 1$ and $\bar{n} \ll 1$ for $p = 1.0$). Regions of negative D correspond to overdamped dynamics; those of positive D correspond to underdamped dynamics.

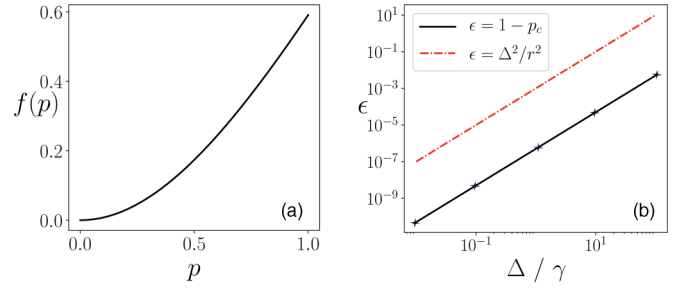


FIG. 4. (a) The universal function $f(p)$ that defines the boundary between the underdamped and overdamped regimes of the strongly driven V-type system. (b) $\epsilon = 1 - p_c$ (solid black line) as a function of Δ/γ for $\bar{n} = 10^3$ with $p_c = \sqrt{1 - \Delta^2/r^2} \simeq 1 - \frac{1}{2} \frac{\Delta^2}{r^2}$ in the overdamped limit. The value of $\epsilon = 1 - p_c$ (dashed red line) predicted by the effective decoherence rate model (Sec. IID) for the same value of \bar{n} .

and the overdamped regime occurs for $\Delta/(\bar{n}\gamma) < 0.6$. As the transition dipoles get out of alignment, the function $f(p)$ decreases, and smaller values of Δ are needed to reach the overdamped regime for a given \bar{n} . For instance, at $p = 1/2$ the overdamped regime is reached for $\Delta/(\bar{n}\gamma) < 0.16$ as illustrated in Fig. 2(a), which shows that the slopes of the $D = 0$ lines decrease proportionally to p .

Figures 2(a) and 2(b) show that the overdamped regime becomes progressively more widespread with increasing the pumping intensity \bar{n} . For large values of $p \simeq 1$ and $\bar{n} \gg 10$ of interest here, the underdamped regime is reached only at very large excited-state splittings ($\Delta/\gamma \gg 10$). In contrast, incoherent excitation of large molecules with dense spectra of rovibrational levels [13] and quantum heat engines [11,12] typically occurs in the small level spacing regime $\Delta/\gamma \ll 1$. This is the regime we will consider in the remainder of this paper.

As shown in Fig. 2(b), the zero- D lines approach constant values $\Delta/p\gamma$ in the weak pumping limit ($\bar{n} \rightarrow 0$). This implies that in this limit, the boundary between the overdamped and underdamped dynamical regimes is defined by the condition $\Delta/p\gamma = 1$, which is consistent with our previous results [13,14]. It is worth observing that the zero- D lines in Fig. 2(b) curve downward as \bar{n} increases from zero to $\bar{n} \sim 0.01$. The reason for this is that the linear term ($d_1\bar{n}$) in Eq. (8) becomes negligible compared to the zeroth- and second-order terms and the discriminant is given by $D = \frac{\gamma^6}{108}(d_0 + d_2\bar{n}^2)$. At higher values of $\bar{n} \sim 0.1$, the zero- D lines reach a minimum and then start to approach their large- \bar{n} limiting values as discussed above.

C. Eigenvalues and coherence lifetimes

As discussed in Sec. II A, in order to obtain the general solution of the BR equations (5), it is necessary to find the exponent of the coefficient matrix \mathbf{A} . To this end, we first diagonalize \mathbf{A} to obtain the eigenvalues λ_k , which give the inverse lifetimes (or decay rates) of the corresponding normal modes \mathbf{V}_k [13,14]. Expanding the characteristic equation for \mathbf{A} in terms of the small parameter $x = \gamma/r = 1/\bar{n}$ (see the

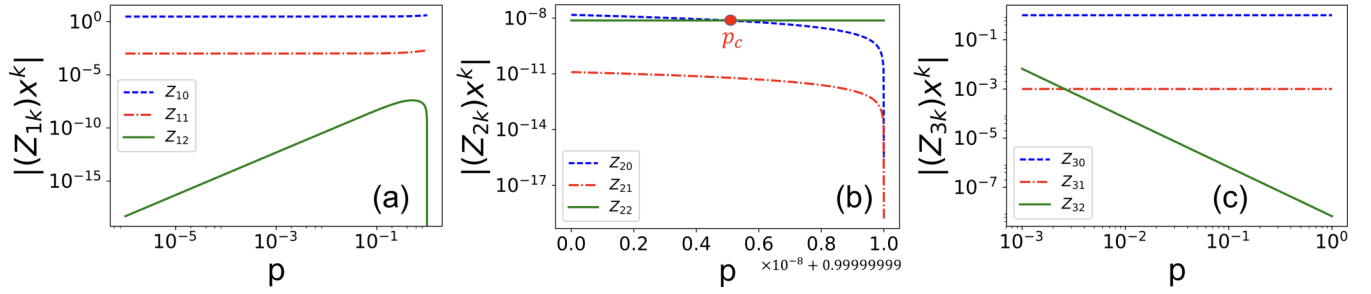


FIG. 5. Relative contributions of the different terms to the eigenvalues λ_1 (a), λ_2 (b), and λ_3 (c) plotted as a function of p for $\Delta/\gamma = 10^{-1}$, $\bar{n} = 10^3$. The absolute values of $z_{jk}x^k$ are plotted because the z_{jk} can take negative values. The nonstandard notation in (b) is used to represent values of p very close to unity, i.e., $0.5 \times 10^{-8} + 0.99999999 = 0.999999995$.

Appendix) we obtain the eigenvalues as

$$\lambda_j = r \sum_{k=0}^8 z_{jk} x^k \quad (j = 1, 2, 3). \quad (9)$$

This expansion is valid for $x \leq 0.01$ and $p > 0.1$ (for $\Delta/\gamma < 1$) and $0.89 < p < 1$ (for $\Delta/\gamma > 1$).

In the overdamped regime, where $\frac{\Delta}{\gamma \bar{n}} \ll f(p)$, the expansion (9) converges rapidly. Keeping the lowest-order terms, we find to excellent accuracy

$$\lambda_j = r[z_{j0} + z_{j1}x + z_{j2}x^2], \quad (10)$$

where the expressions for the coefficients z_{jk} in terms of the system parameters p , Δ/γ , and \bar{n} are (see the Appendix)

$$K = \sqrt[3]{\frac{(8 + 27p^2)}{27} + \sqrt{\frac{p^4(1 + 3p^2)}{3}}} i,$$

$$z_{j0}(p) = \frac{5}{3} - \frac{\alpha_j}{3K} \left(\frac{4}{3} + 3p^2 \right) - \beta_j K,$$

$$z_{j1}(p) = -1 - \frac{\alpha_j}{3K} 4p^2 + \left[\frac{\alpha_j}{3K} \left(\frac{4}{3} + 3p^2 \right) - \beta_j K \right] v_1,$$

$$z_{j2}(p) = f_{j1}(p) \left(\frac{\Delta}{\gamma} \right)^2 + f_{j2}(p), \quad (11)$$

and the parameters K , v_1 , and $f_{jk}(p)$ are listed in Tables I, II, and IV of the Appendix. Here α_j and β_j are the cube roots of unity with values $(\alpha_1, \beta_1) = (1, 1)$, $(\alpha_2, \beta_2) = (\omega^2, \omega)$, $(\alpha_3, \beta_3) = (\omega, \omega^2)$ with $\omega = \frac{(-1+i\sqrt{3})}{2}$ and $\omega^2 = \frac{(-1-i\sqrt{3})}{2}$. Note that since these parameters depend on p only, the coefficients z_{j1} and z_{j0} are independent of the ratio of the excited-state splitting to the radiative decay rate Δ/γ . In contrast, the coefficient of x^2 in Eq. (10) carries an explicit quadratic dependence on Δ/γ .

In order to compare the relative importance of the different terms in Eq. (10), we plot in Fig. 5 the p dependence of $|z_{jk}x^k|$ for $k = 0-2$. Figures 5(a) and 5(c) show that z_{10} provides the dominant contribution to λ_1 and z_{30} provides the dominant contribution to λ_3 for all p , and we can thus approximate

$$\lambda_j = rz_{j0} = (\gamma z_{j0}) \bar{n} \quad (j = 1, 3), \quad (12)$$

where $z_{j0}(p)$ are given by Eq. (11). The scaling behavior given by Eq. (12) is illustrated in Fig. 6(b), which shows that the eigenvalues λ_1 and λ_3 are independent of Δ/γ regardless of the value of p .

Remarkably, however, this is not the case for the eigenvalue λ_2 : As shown in Fig. 5(b) there is a critical value of $p = p_c$ at which the curves $z_{20}(p)$ and $z_{22}(p)x^2$ cross and the relative contributions of the different terms to λ_2 change dramatically. At $p < p_c$, $z_{20}(p)$ is the dominating term so λ_2 scales in the same way as the other eigenvalues (12). For $p > p_c$, the leading term is $z_{22}x^2$ and hence the scaling of λ_2 with Δ/γ is quadratic, the same as that of z_{22} [see Eq. (11)]. The critical value of p depends on Δ/γ and \bar{n} and ranges from 0.995 to 1.0 for $\bar{n} = 10^3$ and $\Delta/\gamma = 10^2-10^{-2}$ [see Fig. 4(b)]. The remarkable sensitivity of the second eigenvalue to the transition dipole alignment parameter p shown in Fig. 5(c) leads to qualitatively different population and coherence dynamics for $p < p_c$ and $p > p_c$ as shown below.

At $p > p_c$, the quadratic contribution to the second eigenvalue is much larger than the linear and constant terms, and hence $\lambda_2 \simeq rz_{22}(\gamma/r)^2$. Combining Eqs. (10) and (11) and noting that $f_{22}(p) \rightarrow 0$ for $p > p_c$, we find

$$\lambda_2 = \frac{\gamma}{\bar{n}} f_{21}(p) \left(\frac{\Delta}{\gamma} \right)^2. \quad (13)$$

The distinct quadratic scaling of λ_2 with Δ/γ is illustrated in Fig. 6(a). The function $f_{21}(p)$ (see the Appendix) increases monotonously approaching the value -0.749 in the limit $p \rightarrow 1$. As the second eigenvalue gives the decay rate of the real part of the coherence (see Sec. II A) the coherence lifetime $\tau_c = 1/|\lambda_2|$ is given by

$$\tau_c = 1.34 \frac{\bar{n}}{\gamma} \left(\frac{\Delta}{\gamma} \right)^{-2} \quad (p > p_c). \quad (14)$$

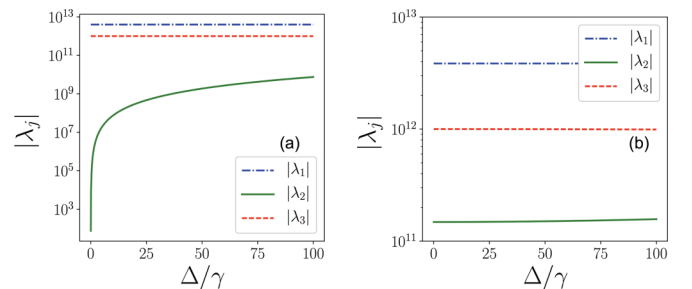


FIG. 6. (a) The eigenvalues λ_j ($j = 1-3$) of matrix **A** plotted vs Δ/γ for $\bar{n} = 10^3$ and $p = 1$. (b) Same as in (a) but for $\bar{n} = 10^3$ and $p = 0.9$.

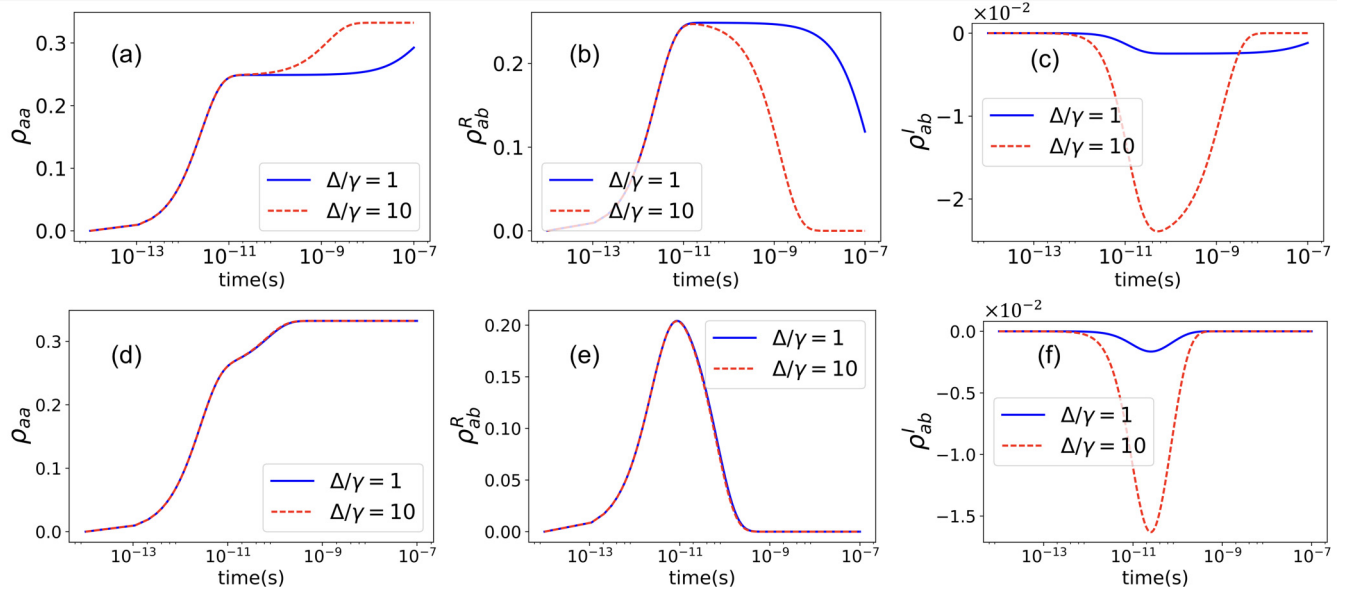


FIG. 7. Excited-state population [(a) and (d)] and coherence [(b), (c), (e), and (f)] dynamics of the symmetric V-type system irradiated by incoherent light for $\bar{n} = 10^2$ and $\Delta/\gamma = 1$ (solid blue line) and 10 (dashed red line). The transition dipole alignment parameter p is set to 1 [(a)–(c)] and to 0.9 [(d)–(f)]. The analytical solutions of the BR equations given by Eqs. (27)–(29) and (30)–(32) (not shown) are indistinguishable from those shown in (a)–(c) and (d)–(f).

Mathematically, the linear scaling of the coherence lifetime is a direct consequence of the second eigenvalue being dominated by a single $z_{22}x^2$ contribution as shown in Fig. 5(b). This characteristic scaling occurs only for $p > p_c$ with $p_c = 1 - \epsilon$ very close to unity [typical values of ϵ range from 5×10^{-11} to 5×10^{-3} for $\bar{n} = 10^3$ as shown in Fig. 4(b)]. Thus, the V-type system with nearly parallel transition dipole moments can exhibit very long coherence times in the strong pumping limit.

For subcritical transition dipole alignment ($p < p_c$), the coherence lifetime becomes

$$\tau_c = \frac{1}{\gamma z_{20}(p)} \bar{n}^{-1} \quad (p < p_c). \quad (15)$$

The coherence lifetimes thus become shorter with increasing the pumping intensity, in stark contrast with the situation in the supercritical regime ($p > p_c$), where the lifetimes increase linearly with \bar{n} (14). Since $z_{20}(p)$ is independent of Δ/γ , the coherence lifetime in the subcritical regime is insensitive to the excited state level splitting.

Figures 7 and 8 illustrate the different regimes of strongly driven coherent dynamics as a function of the excited-state level splitting Δ/γ , the incoherent pumping rate \bar{n} , and the transition dipole alignment parameter p . In the supercritical regime ($p > p_c$) the real and imaginary coherences approach a constant “plateau” value before decaying to zero. Figures 7(b), 7(c) and 8 show that the lifetime of the long-lived coherent state increases with \bar{n} and decreases with Δ/γ in accordance with Eq. (14). Remarkably, the population dynamics shown in Fig. 7(a) reaches a long-lived quasisteady state, in which the populations of the excited levels ($\rho_{aa} = 1/4$) are different from those in thermal equilibrium ($\rho_{aa} = 1/3$). As discussed in more detail in Sec. III B, the lifetime of the quasisteady state is the same as that of the coherences in Eq. (14). Figures 7(b) and 7(c) show that in the supercritical regime ($p > p_c$), the

coherence lifetime τ_c increases linearly with \bar{n} and decreases proportionally to $(\Delta/\gamma)^2$ as given by Eq. (15). The coherence dynamics in the subcritical regime depicted in the bottom panels of Figs. 7 and 8 is in sharp contrast with that in the supercritical regime (top panels of Figs. 7 and 8). We observe that the coherence lifetime calculated for $p < p_c$ actually *decreases* with \bar{n} and becomes insensitive to Δ/γ as predicted by Eq. (15). In the following, we will first analyze the physical reason behind these surprisingly different regimes of coherent dynamics, and then return to the discussion of populations, coherences, and quasisteady states in Sec. III.

D. Physical basis for long-lived Fano coherences: The effective decoherence rate model

To clarify the physical origin of the long coherence times observed in Figs. 7 and 8, consider the competition between the various generation and decay processes described by the BR master equations (1). First, we note that in the strong-pumping limit, incoherent excitation occurs much faster than spontaneous decay ($r \gg \gamma$), so we can neglect the terms proportional to γ to obtain the following simplified system of BR equations for the real and imaginary parts of the Fano coherence $\rho_{ab} = \rho_{ab}^R + i\rho_{ab}^I$,

$$\dot{\rho}_{ab}^R = -r\rho_{ab}^R + pr(\rho_{cc} - \rho_{aa}) + \rho_{ab}^I\Delta, \quad (16)$$

$$\dot{\rho}_{ab}^I = -r\rho_{ab}^I - \rho_{ab}^R\Delta. \quad (17)$$

These equations describe the production and decay of Fano coherences ρ_{ab} due to quantum interference between the incoherent excitation pathways $c \rightarrow a$ and $c \rightarrow b$ originating from the ground state [23–25]. The coherence generation rate $pr\rho_{cc}$ is proportional to the transition dipole alignment parameter p [23,24], which quantifies the extent of interference

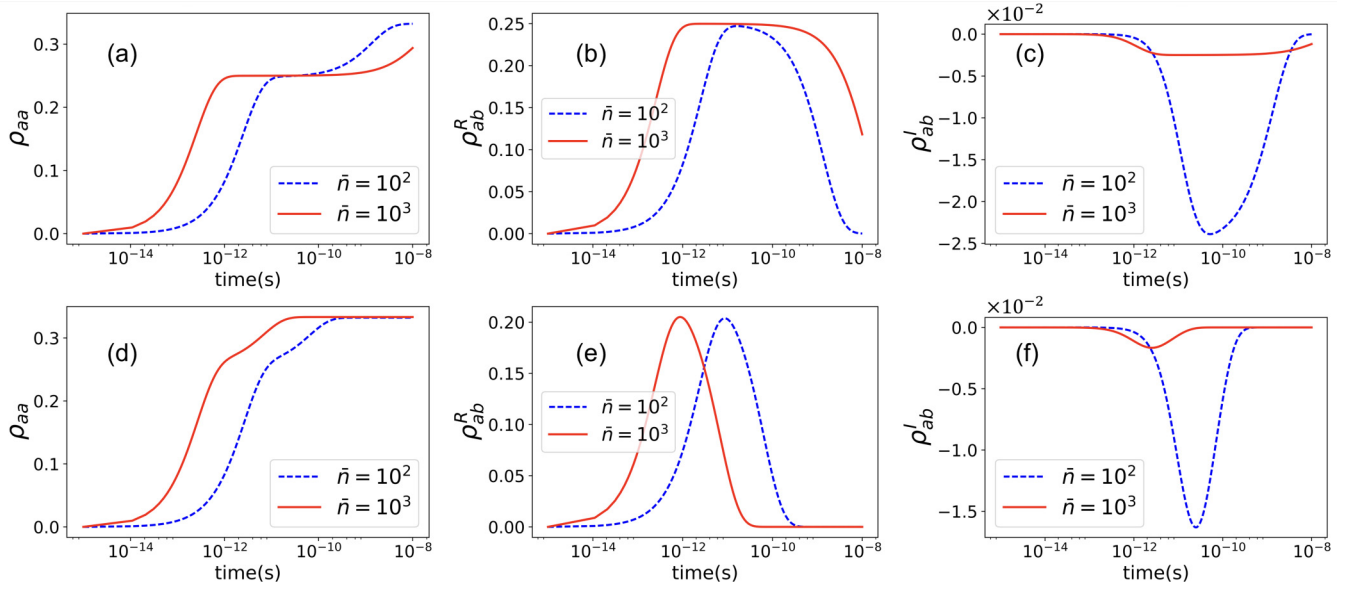


FIG. 8. Excited-state population [(a) and (d)] and coherence [(b), (c), (e), and (f)] dynamics of the symmetric V-type system irradiated by incoherent light for $\bar{n} = 10^3$ (solid red line), $\bar{n} = 10^2$ (dashed blue line), and $\Delta/\gamma = 10$. The transition dipole alignment parameter p is set to 1 [(a)–(c)] and to 0.9 [(d)–(f)]. The analytical solutions of the BR equations given by Eqs. (27)–(29) and (30)–(32) (not shown) are indistinguishable from those shown in (a)–(c) and (d)–(f).

between the two transitions [23,24]. Significantly, only the *real part of the coherence* is generated directly via the interference process. The imaginary coherence is decoupled from the population dynamics to first order, but can still exhibit nontrivial evolution due to coupling to the real coherence through the $\rho_{ab}^R \Delta$ term in Eq. (17). Once generated, the coherences evolve unitarily in time according to the terms proportional to Δ and decay via stimulated emission described by the term $-r\rho_{ab}$. An additional interference term $pr(\rho_{cc} - \rho_{aa})$ in Eq. (16) is proportional to the population difference between the ground and excited levels.

To illustrate the interplay between the coherence-generating and coherence-destroying mechanisms, we plot in Fig. 9 the

time evolution of the populations and coherences that enter Eq. (16). The decay of the ground-state population ρ_{cc} is accompanied by a steady growth of excited-state populations and coherences. In the quasisteady state that is formed on the timescale $1/r < t < \tau_c$ (see above and Sec. III B) the population inversion term $\rho_{cc} - \rho_{aa}$ drives coherence generation. From Fig. 9 we observe that in the quasisteady state (1) the time evolution of the population difference $\rho_{cc} - \rho_{aa}$ is identical to that of the real part of the coherence ρ_{ab}^R and (2) the imaginary part of the coherence remains constant in time. Setting the left-hand side of Eq. (17) to zero, we obtain the imaginary part of the quasisteady coherence as $\rho_{ab}^I = -(\Delta/r)\rho_{ab}^R$ (we verified this result numerically in the overdamped regime). These considerations allow us to simplify Eq. (16) to yield

$$\dot{\rho}_{ab}^R = -r \left(1 - p + \frac{\Delta^2}{r^2} \right) \rho_{ab}^R \quad (t > 1/r), \quad (18)$$

which describes coherence decay on the timescale $t > 1/r$ (note that coherence generation occurs on shorter timescales given by $t \simeq 1/r$). The simple form of Eq. (18) enables us to introduce an *effective decoherence rate* $\gamma_d^{\text{eff}}(p) = r(1 - p + \frac{\Delta^2}{r^2})$ and an *effective coherence lifetime*

$$\tau_d^{\text{eff}} = \frac{1}{r(1 - p + \frac{\Delta^2}{r^2})}. \quad (19)$$

The effective decoherence rate model thus establishes that the lifetime of noise-induced coherences is determined by two mechanisms: (1) the interplay between coherence-generating Fano interference and stimulated decay discussed above [the term $r(1 - p)$] and (2) the coupling between the real and imaginary parts of the coherence (the term Δ^2/r). The second mechanism is due to the unitary interconversion between the real and imaginary parts of the coherence, which occurs at a rate Δ . Because the imaginary coherence decays at a rate r

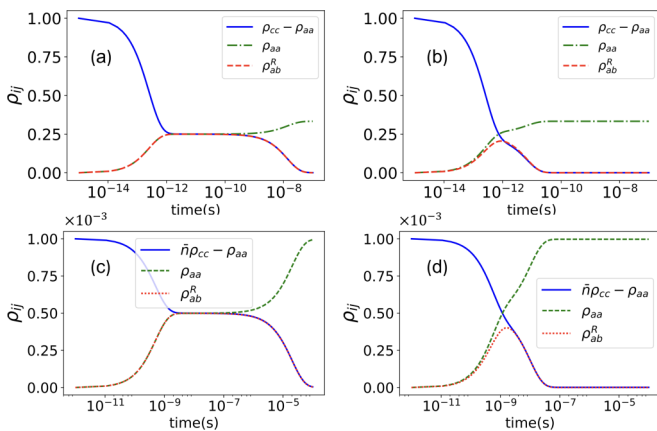


FIG. 9. Population and coherence dynamics of the symmetric V-type system in the strong-pumping limit (upper panels, $\bar{n} = 10^3$) for $\Delta/\gamma = 10$ and in the weak-pumping limit (lower panels, $\bar{n} = 10^{-3}$) for $\Delta/\gamma = 10^{-2}$. The transition dipole alignment parameter p is set to 1 [(a) and (c)] and to 0.9 [(b) and (d)].

[Eq. (17)], this unitary interconversion makes a small second-order contribution to the overall decay rate proportional to Δ^2 . The two mechanisms contribute equally for $p = p_c^{\text{eff}}$ where

$$p_c^{\text{eff}} = 1 - \frac{\Delta^2}{r^2}, \quad (20)$$

which is not too far from the exact result shown in Fig. 4(b).

Our expression for the effective coherence lifetime (19) clarifies the physical origin of the different regimes of coherent dynamics discussed in the previous section. At $p > p_c^{\text{eff}}$ the term $r(1-p)$ is small compared with Δ^2/r , the rate of coherence generation (via Fano interference) and decay (via incoherent stimulated emission) are almost exactly balanced. As a result, the effective decoherence rate is dominated by the second-order mechanism (2) and Eq. (19) yields $\tau_d^{\text{eff}} = r/\Delta^2 = \bar{n}\gamma/\Delta^2$, which is identical to the exact result (14) to within the factor 1.34. Remarkably, the effective decoherence rate model correctly predicts the linear scaling of the coherence lifetime with both \bar{n} and Δ/γ in the $p > p_c$ regime.

At $p < p_c^{\text{eff}}$, the rate of coherence decay exceeds that of coherence generation, the term $r(1-p)$ dominates, and the effective coherence time is determined by the interplay between Fano interference and stimulated decay. From Eq. (19) we obtain $\tau_d^{\text{eff}} = \frac{1}{r(1-p)}$, again consistent with the exact result (15) to within a numerical factor. As in the limit $p \rightarrow 1$, the effective decoherence model correctly predicts the inverse scaling of the coherence lifetime with \bar{n} in the $p < p_c$ regime.

In closing, we note that in view of Eq. (19) the transition dipole alignment parameter p can be thought of as controlling the relative contribution of mechanisms (1) and (2) to the overall effective decoherence rate (19). In the strong-pumping regime of interest here, mechanism (1) is much more efficient in destroying the coherence than mechanism (2). Fortunately, mechanism (1) is p dependent and can be suppressed by taking $p \rightarrow 1$, leading to the long-lived coherent regime governed by mechanism (2).

E. Comparison with the weak-pumping limit

It is instructive to compare the coherence time of the V-type system in the strong-pumping and weak-pumping regimes. In the small level spacing regime ($\Delta/\gamma < 1$), the coherence time under weak pumping [13,14]

$$\tau_c^{\text{WP}} = \frac{2}{\gamma} \left(\frac{\Delta}{\gamma} \right)^{-2} \quad (21)$$

exhibits the same $(\Delta/\gamma)^{-2}$ scaling as in the strong-pumping regime [13,14], becoming longer as the excited-state energy gap Δ narrows down. The ratio of the coherence times in the strong- and weak-pumping limits is thus, for $p > p_c$,

$$\frac{\tau_c}{\tau_c^{\text{WP}}} \simeq 0.67\bar{n}. \quad (22)$$

The enhancement of the coherence lifetime under strong pumping ($\bar{n} > 1.5$) may facilitate the experimental observation of the noise-induced coherences in atomic systems [26].

We now apply the effective decoherence rate model in the weak-pumping limit, where the BR equation

$$\dot{\rho}_{ab} = p\gamma(\bar{n}\rho_{cc} - \rho_{aa}) - \gamma\rho_{ab} + i\Delta\rho_{ab} \quad (23)$$

can be simplified to give for $t > 1/\gamma$,

$$\dot{\rho}_{ab}^R = - \left[(1-p)\gamma + \frac{\Delta^2}{\gamma} \right] \rho_{ab}^R, \quad (24)$$

Here we used the relation between the real and imaginary coherences in the quasisteady state $\rho_{ab}^I = -(\Delta/\gamma)\rho_{ab}^R$ and the relationship $\bar{n}\rho_{cc} - \rho_{aa} = \rho_{ab}^R$ illustrated in Fig. 9(c). The coherence time in the weak-pumping limit immediately follows from Eq. (24),

$$\tau_c^{\text{WP}} = \frac{1}{\gamma(1-p) + \frac{\Delta^2}{\gamma}}. \quad (25)$$

The effective decoherence rate is composed of contributions due to (1) the interplay between Fano interference and spontaneous decay and (2) the coupling between the real and imaginary parts of the coherence. This is similar to the strong pumping case considered in Sec. IID; the only difference is that mechanism (1) is due to spontaneous, rather than stimulated decay. The relative importance of mechanisms (1) and (2) depends on the value of p . At $p > p_c^{\text{WP}}$ the second contribution dominates, and Eq. (25) gives $\tau_c = \gamma/\Delta^2$ in agreement with our previous result (21) to within a factor of 2 [13,14]. At $p < p_c$ the first contribution dominates and the coherence time is given by $1/(1-p)\gamma$. The transition between the two regimes occurs at $p_c^{\text{WP}} = 1 - \Delta^2/\gamma^2$, which is close to the exact value $p_c^{\text{WP}} = \sqrt{1 - \Delta^2/\gamma^2} \simeq 1 - \frac{\Delta^2}{2\gamma^2}$ [14]. Note that in the overdamped regime of the weakly driven V-type system ($\Delta/\gamma \ll 1$ [13,14]) the value of p_c is very close to unity, reflecting the dominance of the spontaneous decay mechanism represented by the term $\gamma(1-p)$ over the second-order coherence transfer mechanism represented by the term Δ^2/γ over much of the p range. This is similar to the situation encountered for the strongly driven V-type system, where the competing mechanisms are stimulated decay and second-order coherence transfer.

III. POPULATION AND COHERENCE DYNAMICS

A. Analytic solutions in the overdamped regime

$$[\Delta/(\bar{n}\gamma) < f(p)]$$

Having classified the dynamical regimes of the strongly driven V-type system and analyzed the relevant eigenmodes, we now turn to the time evolution of the density matrix elements. From Eq. (5), we obtain as shown in the Appendix

$$\rho_{ij}(t) = \frac{r}{\det(\mathbf{M})} \sum_{k=1}^3 \frac{(e^{\lambda_k t} - 1)}{\lambda_k} V_{k,n(i,j)} (T_{k1} + pT_{k2}), \quad (26)$$

where $n(i,j) = 1$ for the excited-state population ($i = j = a$) and $n(i,j) = 2(3)$ for the real (imaginary) part of the two-photon coherence ($i = a, j = b$). The density matrix elements in Eq. (26) are expressed as a linear combination of exponentially decaying terms, weighted with the components V_{kj} of eigenvectors of \mathbf{A} (which form the fundamental matrix \mathbf{M}) and the elements of its adjoint matrix T_{kj} , which depend on p only.

To express the density matrix dynamics in terms of the physical parameters Δ/γ , \bar{n} , and p , we evaluate the eigenvector components V_{kj} and T_{kj} in Eq. (26) as described in the Appendix and use the resulting expressions in Eq. (5) to obtain

for $p > p_c$,

$$\rho_{aa}(t) = \frac{1}{[-4 + 1.33 \frac{1}{\bar{n}^2} (\frac{\Delta}{\gamma})^2]} \left\{ \left[-4 + 2.92 \frac{1}{\bar{n}^2} \left(\frac{\Delta}{\gamma} \right)^2 \right] \frac{(1 - e^{-4\gamma \bar{n}t})}{4} - \frac{(1 - e^{-0.75 \frac{\gamma}{\bar{n}} (\frac{\Delta}{\gamma})^2 t})}{3} + 0.44 \frac{1}{\bar{n}^2} \left(\frac{\Delta}{\gamma} \right)^2 (1 - e^{-\gamma \bar{n}t}) \right\}, \quad (27)$$

$$\rho_{ab}^R(t) = \frac{1}{[-4 + 1.33 \frac{1}{\bar{n}^2} (\frac{\Delta}{\gamma})^2]} \left\{ \left[-4 + 3.249 \frac{1}{\bar{n}^2} \left(\frac{\Delta}{\gamma} \right)^2 \right] \frac{(1 - e^{-4\gamma \bar{n}t})}{4} + (1 - e^{-0.75 \frac{\gamma}{\bar{n}} (\frac{\Delta}{\gamma})^2 t}) - 0.89 \frac{1}{\bar{n}^2} \left(\frac{\Delta}{\gamma} \right)^2 (1 - e^{-\gamma \bar{n}t}) \right\}, \quad (28)$$

$$\rho_{ab}^I(t) = \frac{1}{[-4 + 1.33 \frac{1}{\bar{n}^2} (\frac{\Delta}{\gamma})^2]} \frac{1}{\bar{n}} \left(\frac{\Delta}{\gamma} \right) \left\{ \left[-1.33 + 0.99 \frac{1}{\bar{n}^2} \left(\frac{\Delta}{\gamma} \right)^2 \right] \frac{(1 - e^{-4\gamma \bar{n}t})}{4} - (1 - e^{-0.75 \frac{\gamma}{\bar{n}} (\frac{\Delta}{\gamma})^2 t}) + \left[1.33 - 0.25 \frac{1}{\bar{n}^2} \left(\frac{\Delta}{\gamma} \right)^2 \right] (1 - e^{-\gamma \bar{n}t}) \right\}. \quad (29)$$

The second term on the right-hand-side of Eq. (28) represents the slowly decaying coherent mode, the eigenvector of the coefficient matrix \mathbf{A} corresponding to the eigenvalue λ_2 which gives the decay rate of the real part of coherence. As discussed below, this coherent mode also manifests itself in the time evolution of excited-state populations (27). The lifetime of the coherent mode scales as $\bar{n}(\Delta/\gamma)^{-2}$, leading to arbitrarily long coherence lifetimes for small excited-state splittings. In contrast, the first and third terms on the right-hand side of Eqs. (27)–(29) decay much faster, with lifetimes proportional to $1/\bar{n}$.

For subcritical transition dipole alignment ($p < p_c$) the population and coherence dynamics take the form

$$\rho_{aa}(t) = \frac{1}{D} \left\{ \sum_{k=1}^2 A_{2k-1}(p) \frac{1 - e^{-\gamma |z_{k0}| \bar{n}t}}{|z_{k0}|} + \frac{1}{\bar{n}^2} \left(\frac{\Delta}{\gamma} \right)^2 \left[\sum_{k=1}^2 A_{2k}(p) \frac{1 - e^{-\gamma |z_{k0}| \bar{n}t}}{|z_{k0}|} + A_5 \frac{1 - e^{-\gamma |z_{30}| \bar{n}t}}{|z_{30}|} \right] \right\}, \quad (30)$$

$$\rho_{ab}^R(t) = \frac{1}{D} \left\{ \sum_{k=1}^2 B_{2k-1}(p) \frac{1 - e^{-\gamma |z_{k0}| \bar{n}t}}{|z_{k0}|} + \frac{1}{\bar{n}^2} \left(\frac{\Delta}{\gamma} \right)^2 \left[\sum_{k=1}^2 B_{2k}(p) \frac{1 - e^{-\gamma |z_{k0}| \bar{n}t}}{|z_{k0}|} + B_5 \frac{1 - e^{-\gamma |z_{30}| \bar{n}t}}{|z_{30}|} \right] \right\}, \quad (31)$$

$$\rho_{ab}^I(t) = \frac{1}{D} \frac{1}{\bar{n}} \left(\frac{\Delta}{\gamma} \right) \left\{ \sum_{k=1}^3 C_{2k-1}(p) \frac{1 - e^{-\gamma |z_{k0}| \bar{n}t}}{|z_{k0}|} + \frac{1}{\bar{n}^2} \left(\frac{\Delta}{\gamma} \right)^2 \sum_{k=1}^3 C_{2k}(p) \frac{1 - e^{-\gamma |z_{k0}| \bar{n}t}}{|z_{k0}|} \right\}, \quad (32)$$

where $D = T_1(p) + T_2(p) \frac{1}{\bar{n}^2} (\frac{\Delta}{\gamma})^2$ and the coefficients $A_i(p)$, $B_i(p)$, and $C_i(p)$ are plotted in Fig. 10 as a function of p . Note that, in contrast to the $p > p_c$ case considered above, all of the exponential terms on the right-hand side of Eqs. (30)–(32) scale linearly with \bar{n} and are independent of Δ/γ (see Sec. IIB). The coherence dynamics given by Eqs. (30)–(32) is thus much more short lived than that observed in the case of nearly parallel transition dipole moments.

Our analytical results (30)–(32) for the time evolution of the populations and coherences are identical to the numerical solutions of the BR equations (1) shown in Figs 7 and 8. A sudden turn-on of incoherent pumping at $t = 0$ initiates population transfer from the ground state to the excited eigenstates and generates two-photon coherences among them. The excited-state populations reach a plateau and then grow monotonously to their equilibrium steady-state values $\rho_{aa} = \rho_{bb} = \rho_{gg} = 1/3$ as discussed in detail in the following section.

The real and imaginary parts of the two-photon coherence shown in Figs. 7(b) and 7(c) grow monotonously, reaching a plateau on the timescale $t \sim 1/r = \bar{n}\gamma$ and then surviving for the duration τ_c of the coherence lifetime given by Eq. (14). By comparing Figs. 7(b) and 7(e), we observe that the coherences become much more short lived for subcritical transition dipole

alignment ($p < p_c$) in accordance with Eqs. (14) and (15). In the limit $t \gg \tau_c$ the coherences decay to zero and the V-type system reaches the expected thermal equilibrium state [8].

B. Analytic solutions for closely spaced levels [$\Delta/\gamma \ll 1$]

Our analytical expressions for the population and coherence dynamics (27)–(29) and (30)–(32) are valid in the overdamped regime defined by the condition $\Delta/(\bar{n}\gamma) < f(p)$. Since $\bar{n} \gg 1$, the condition $\Delta/(\bar{n}\gamma) < f(p)$ does not necessarily imply that the excited-state splittings should be small compared to the radiative decay rate (i.e., $\Delta/\gamma \ll 1$). As a result, the strongly driven V-type system can exhibit overdamped coherent behavior even when the excited-state level splitting is large compared to the natural linewidth ($\Delta/\gamma \gg 1$) provided that $\Delta/\gamma < f(p)\bar{n}$. Nevertheless, major simplifications are possible in the limit of closely spaced excited-state levels ($\Delta/\gamma \ll 1$), which is of special interest for incoherent excitation of large molecules [13]. It is also in this limit that the weakly driven V-type system exhibits long-lived coherences [13,14].

Neglecting the terms proportional to $(\Delta/\gamma)^2$ in Eqs. (27)–(29) and replacing the p -dependent coefficients z_{jk} , $|f_{21}(p)|$, $A_i(p)$, $B_i(p)$, and $C_i(p)$ (see Fig. 10) by their values at $p = 1$, we obtain for nearly parallel transition dipole

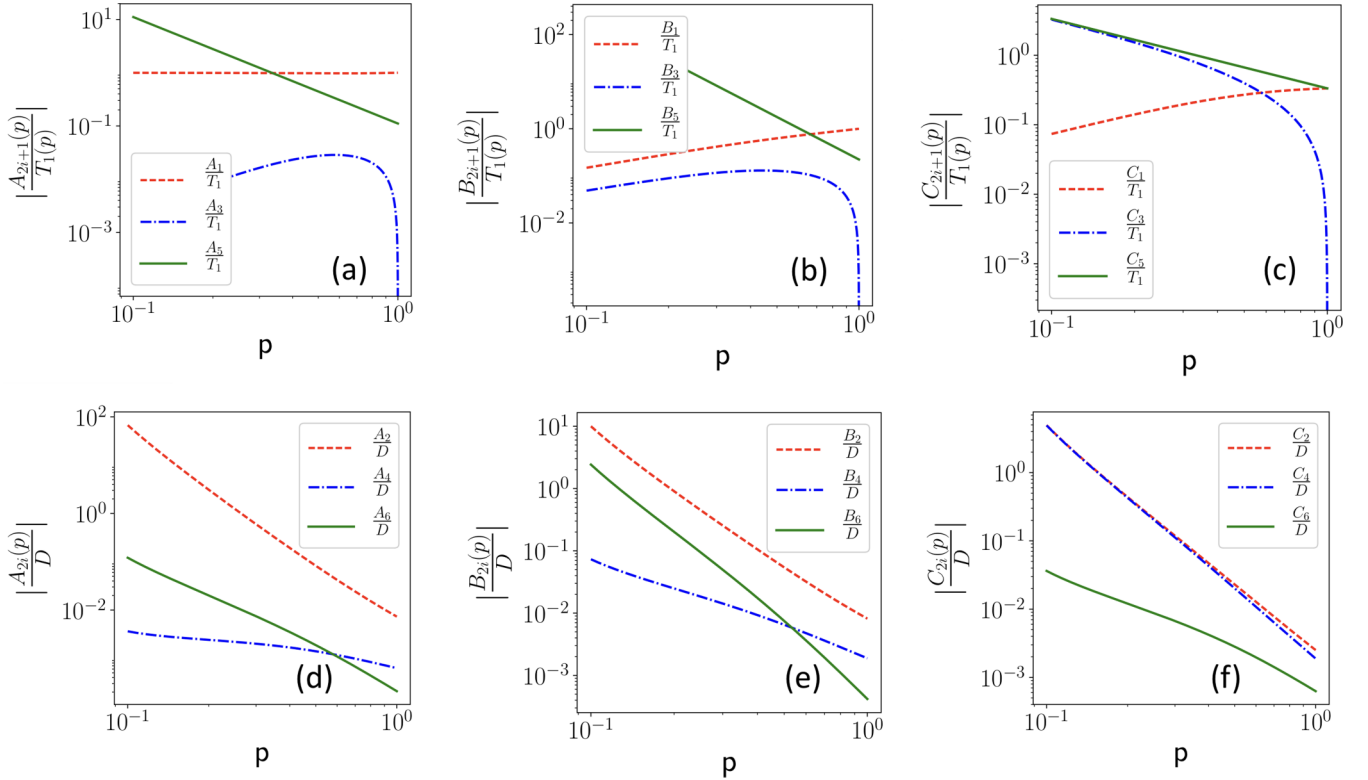


FIG. 10. (Upper panels) Normalized contributions $A_{2i+1}/T_1(p)$, $B_{2i+1}/T_1(p)$, and $C_{2i+1}/T_1(p)$ ($i = 1-3$) to $\rho_{aa}(t)$ (a), $\rho_{ab}^R(t)$ (b), and $\rho_{ab}^I(t)$ (c) plotted as a function of p for $\frac{\Delta}{\gamma} \ll 1$. (Lower panels) Normalized contributions A_{2i} , B_{2i} , C_{2i} ($i = 1-3$) to $\rho_{aa}(t)$ (d), $\rho_{ab}^R(t)$ (e), and $\rho_{ab}^I(t)$ (f) plotted as a function of p for $\bar{n} = 10^3$, $\frac{\Delta}{\gamma} = 10^2$. The normalization factor $D = [T_1(p) + T_2(p)\frac{1}{\bar{n}}(\frac{\Delta}{\gamma})^2]$.

moments ($p > p_c$)

$$\rho_{aa}(t) = \frac{1}{3} - \frac{1}{12}(3e^{-4\gamma\bar{n}t} + e^{-0.75\frac{\Delta}{\bar{n}}(\frac{\Delta}{\gamma})^2t}), \quad (33)$$

$$\rho_{ab}^R(t) = \frac{1}{4}(e^{-0.75\frac{\Delta}{\bar{n}}(\frac{\Delta}{\gamma})^2t} - e^{-4\gamma\bar{n}t}), \quad (34)$$

$$\rho_{ab}^I(t) = -\frac{1}{12}\left(\frac{\Delta}{\bar{n}\gamma}\right)(e^{-4\gamma\bar{n}t} + 3e^{-0.75\frac{\Delta}{\bar{n}}(\frac{\Delta}{\gamma})^2t} - 4e^{-\gamma\bar{n}t}). \quad (35)$$

These expressions clearly establish the existence of two vastly different timescales of coherent dynamics. As shown in Fig. 7(b), at very short times ($t < \frac{1}{4\gamma\bar{n}}$) the real part of the coherence increases to its quasisteady value of $\frac{1}{4}$ and then survives for a long time τ_c (14) due to the second term on the right-hand side of Eq. (34), which eventually decays to zero for $t \gg \frac{\bar{n}}{\gamma}(\frac{\Delta}{\gamma})^{-2}$. Figures 7(b) and 8(b) illustrate that noise-induced coherences in the supercritical regime ($p > p_c$) become more long lived with increasing the pumping intensity \bar{n} and decreasing the excited state splitting Δ in agreement with Eqs. (14) and (34). As pointed out in Sec. IID, the physical reason behind this scaling is that the decoherence mechanism (2) involves interconversion between the real and imaginary parts of the coherence, which slows down with decreasing Δ . Figure 7(c) shows that the imaginary part of the coherence, while also lasting for a long time, is suppressed by the factor ($\frac{\Delta}{\bar{n}\gamma} \ll 1$) as previously found in the weak-pumping limit [13,14].

We now turn to the time evolution of excited-state populations (35) displayed in Figs. 7(a) and 8(a), which is in good agreement with exact numerical solutions of the BR equations. At $p > p_c$ the populations grow monotonously on the timescale $t < 1/4(\bar{n}\gamma)$ to reach their plateau values $\rho_{aa} = \rho_{bb} = \frac{1}{4}$. As these values are different from those expected in thermal equilibrium ($\rho_{ii} = 1/3$) this signals the formation of a long-lived *quasisteady state* featuring significant coherences in the energy eigenstate basis, which slows down the process of thermalization of the V-type system with the bath. In fact, as shown in Figs. 7(a) and 8(a) full thermalization does not occur until after $t \gg \tau_c$ when the populations reach their equilibrium values of $1/3$ and the quasisteady state decays into an incoherent mixture of eigenstates. This is consistent with the previous results of Agarwal and Menon, who showed that the long-time evolution of the BR equations always leads to a coherence-free steady state [8].

The physical origin of the slow thermalization illustrated in Figs. 7(a) and 8(a) is directly related to the long-lived Fano coherences generated in the $p > p_c$ regime. Indeed, it follows from Eq. (1) that excited-state populations decay faster in the presence of Fano coherence due to the interference-mediated coupling between the populations and coherences given by the last term on the right-hand side of Eq. (1). As a result of this additional decay channel, the values of excited-state populations are smaller than those in thermal equilibrium as long as $\rho_{ab}^R > 0$, i.e., during the lifetime of the quasisteady state [see Eq. (14)].

For the subcritical regime ($p < p_c$) we find

$$\rho_{aa}(t) = \frac{1}{T_1(p)} \left\{ A_1 \left(\frac{1 - e^{-\gamma|z_{10}|\bar{n}t}}{|z_{10}|} \right) + A_3 \left(\frac{1 - e^{-\gamma|z_{20}|\bar{n}t}}{|z_{20}|} \right) \right\}, \quad (36)$$

$$\rho_{ab}^R(t) = \frac{1}{T_1(p)} \left\{ B_1 \left(\frac{1 - e^{-\gamma|z_{10}|\bar{n}t}}{|z_{10}|} \right) + B_3 \left(\frac{1 - e^{-\gamma|z_{20}|\bar{n}t}}{|z_{20}|} \right) \right\}, \quad (37)$$

$$\rho_{ab}^I(t) = \frac{1}{T_1(p)} \left(\frac{\Delta}{\bar{n}\gamma} \right) \left\{ C_1 \left(\frac{1 - e^{-\gamma|z_{10}|\bar{n}t}}{|z_{10}|} \right) + C_3 \left(\frac{1 - e^{-\gamma|z_{20}|\bar{n}t}}{|z_{20}|} \right) + C_5 \left(\frac{1 - e^{-\gamma|z_{30}|\bar{n}t}}{|z_{30}|} \right) \right\}. \quad (38)$$

These analytical solutions are in excellent agreement with numerical results shown in the lower panels of Figs. 7 and 8. The population and coherence dynamics do not exhibit long-lived quasisteady states, and populations reach their equilibrium values on the expected timescale given by Eq. (15). The population and real part of the coherence are independent of the excited state splitting Δ as shown in Figs. 7(d) and 7(e).

Finally, we note that our analytical solutions for the populations (33) and (36) are manifestly positive for the initial conditions studied in this work [$\rho_{cc}(0) = 1$], so the dynamics studied here are not influenced by the artifacts due to nonpositivity that are known to affect the solutions of BR equations in certain regimes [20].

IV. SUMMARY AND CONCLUSIONS

We have studied the quantum dynamics of a three-level V-type system interacting with a thermal environment in a previously unexplored regime, where incoherent pumping occurs much faster than spontaneous emission. This regime is characterized by a large number of thermal bath phonons ($\bar{n} \gg 1$) at the excitation frequency, and it is relevant for artificial solar light harvesting and the design of efficient quantum heat engines [11,12,20,21], of which the V-type system is a key building block.

As a primary tool to study the dynamics of the strongly driven V-type system, we use nonsecular BR equations, which provide a unified description of time-evolving populations and coherences in multilevel quantum systems weakly interacting with a thermal bath. The nonsecular description retains the population-to-coherence coupling terms proportional to the transition dipole alignment factor p , which are essential for a proper description of noise-induced coherences [13]. By examining the discriminant of the characteristic polynomial, we classify the dynamical regimes of the strongly driven V-type system into underdamped, overdamped, and critical (Sec. II A). For large excited-state splittings such that $\Delta/(\bar{n}\gamma) > f(p)$, where $f(p)$ is a universal function of p plotted in Fig. 4, the two-photon coherences show underdamped oscillations. In the overdamped regime of small level spacing [$\Delta/(\bar{n}\gamma) < 1$], the coherences evolve monotonously as a function of time. A remarkable dynamical effect which occurs in this regime is the formation of long-lived, coherent quasisteady states with lifetimes $\tau_c = 1.34(\bar{n}/\gamma)(\Delta/\gamma)^{-2}$ that can be arbitrarily long in V-type systems with vanishingly small level splittings. As illustrated in Figs. 7 and 8, the quasisteady states strongly affect the time evolution of the density matrix elements, enhancing the lifetime of two-photon coherences and slowing down the

approach of excited-state populations to thermodynamic equilibrium. The quasisteady states only form when the transition dipole moments of the V-type system are nearly perfectly aligned.

We further show that in the overdamped regime, the solutions of the BR equations can be represented analytically as a sum of three exponentially decaying terms [see, e.g., Eqs. (27)–(29)]. The behavior of the solutions depends strongly on the transition dipole alignment factor p . For $p > p_c$, the long-lived coherent mode emerges, whereas for $p < p_c$ all modes have comparable lifetimes, which scale as $1/\bar{n}$. Particularly simple expressions (35) are obtained in the limit of small level spacing $\Delta/\gamma \ll 1$. All of the expressions are in excellent agreement with numerical solutions of the BR equations (Figs. 7 and 8).

To clarify the physical origin of the different regimes of noise-induced coherent dynamics, we have developed an effective decoherence rate model, which accounts for the most important coherence-generating and coherence-destroying mechanisms in a V-type system driven by a thermal environment, including Fano interference (which generates the coherences), the decay processes due to stimulated and spontaneous emission, and the interconversion between the real and imaginary part of the coherence followed by an irreversible decay of the latter. In the limit $p \rightarrow 1$ the rate of coherence generation via Fano interference is maximized, approaching that of coherence decay via stimulated and spontaneous emission, so the overall decay is determined by a slow interconversion between the real and imaginary parts of the coherence as described above. This process is suppressed at small Δ leading to very long coherence lifetimes described by the effective decoherence rate model [see Eqs. (19) and (25)]. At $p < 1$ the rate of stimulated and spontaneous decays rapidly exceeds that of coherence generation via Fano interference, and thus the lifetime of the coherences decreases sharply. The nearly perfect alignment of transition dipole moments ($p > p_c$) is thus an essential condition for the longevity of noise-induced coherences in both the weak-pumping and strong-pumping regimes.

Finally, we consider the question of how the long-lived noise-induced coherent effects predicted here could be observed in the laboratory. Such an observation would require an atomic or molecular V-type system with nearly parallel transition dipole moments ($p > p_c$) driven by a bright ($\bar{n} \gg 1$) source of incoherent radiation. For the latter, one can use concentrated solar light (for which $\bar{n} \simeq 10^4$ can be achieved at typical optical frequencies [11,12,21]) or broadband laser radiation [8].

The requirement of nearly perfectly aligned transition dipoles ($p > p_c$) is more restrictive, since the overwhelming

majority of electric dipole transitions to nearly degenerate (V-type systemlike) excited atomic states tend to have $p < 1$ [6,8,13].

To bypass this requirement, we consider incoherent excitation by a linearly polarized blackbody radiation, for which transitions to nearly degenerate upper levels with different projections m_J of the total electronic angular momentum J exhibit Fano interference [8,26].

In future work, we intend to explore the possibility for experimental observation of Fano coherences with highly excited Rydberg atoms. As a consequence of their exaggerated transition dipole moments, Rydberg atoms couple strongly to blackbody radiation, and can therefore be used as an attractive experimental platform to study noise-induced coherence effects [27,28]. Consider, e.g., the $65s$ Rydberg state of atomic Rb interacting with thermal blackbody radiation at $T = 300$ K [28]. The energy splitting ω_{ac} between the initial $65s$ state and the nearby m_J components of the $65p$ state (forming the Rydberg V-type system) is 0.44 cm^{-1} . The average number of thermal photons at this transition frequency is $\bar{n} \sim 400$ [27], putting the Rydberg V-type system in the strong pumping regime. The splitting between the different m_J components of the $65p$ state can be tuned by an external magnetic field to vary the ratio $\Delta/\bar{n}\gamma$, providing access to the different regimes of noise-induced coherent dynamics studied in this work.

Note added in proof. Recent theoretical work has considered quantum coherences in an incoherently driven system of two-level atoms coupled by the dipole-dipole interaction [29,30].

APPENDIX: ANALYTIC EXPRESSIONS

In this Appendix we present a detailed derivation of the analytic expressions for the discriminant \mathcal{D} and the eigenvalues and eigenvectors of the coefficient matrix \mathbf{A} given by Eq. (4) of the main text as a function of the V-type system parameters γ , r , and $\frac{\Delta}{\gamma}$. We also derive the analytic expressions for the populations and coherence dynamics which appear in

Eqs. (27)–(29) and (33)–(35) of the main text. The solutions are expressed in terms of the p -dependent coefficients listed in Tables I–XII.

1. Discriminant of the coefficient matrix \mathbf{A}

The general expression of the discriminant of the coefficient matrix is

$$D = B^3 + \left[C - \frac{3}{2}A(B + A^2) \right]^2, \quad (\text{A1})$$

where

$$A = \frac{1}{3}(5r + 3\gamma), \quad (\text{A2})$$

$$B = \frac{\Delta^2}{3} - \frac{\gamma^2 p^2}{3} + \gamma^2 - \frac{4}{3}\gamma p^2 r + \frac{10}{3}\gamma r - p^2 r^2 + \frac{7}{3}r^2 - \frac{1}{9}(5r + 3\gamma)^2, \quad (\text{A3})$$

$$C = \frac{1}{2}\Delta^2 \gamma + \frac{3}{2}\Delta^2 r - \frac{1}{2}\gamma^3 p^2 + \frac{1}{2}\gamma^3 - \frac{5}{2}r\gamma^2 - \frac{7}{2}\gamma p^2 r^2 + \frac{7}{2}\gamma r^2 - \frac{3}{2}p^2 r^3 + \frac{3}{2}r^3 + \frac{1}{27}(5r + 3\gamma)^3. \quad (\text{A4})$$

It is convenient to express the terms A , B , C as a function of the occupation number \bar{n} ,

$$A = \frac{\gamma}{3}(3 + 5\bar{n}), \quad (\text{A5})$$

$$B = \frac{\gamma^2}{3} \left[\frac{\Delta^2}{\gamma^2} - p^2 - 4p^2 \bar{n} - \left(\frac{4}{3} + 3p^2 \right) \bar{n}^2 \right], \quad (\text{A6})$$

$$C = \frac{\gamma^3}{2} \left[\frac{\Delta^2}{\gamma^2} + (3 - p^2) + \left(15 - 5p^2 + 3\frac{\Delta^2}{\gamma^2} \right) \bar{n} + \left(\frac{71}{3} - 7p^2 \right) \bar{n}^2 + \left(\frac{331}{27} - 3p^2 \right) \bar{n}^3 \right], \quad (\text{A7})$$

$$C - \frac{3}{2}A(B + A^2) = \frac{\gamma^3}{6} \left[\left(4\frac{\Delta^2}{\gamma^2} + 2p^2 \right) \bar{n} + 8p^2 \bar{n}^2 + \frac{(16 + 54p^2)}{9} \bar{n}^3 \right]. \quad (\text{A8})$$

TABLE I. The expansion coefficients c_k , d_k , and b_k for \mathcal{D} , E , and $\beta(x)$.

| c_i | d_i | b_i |
|--|--|---|
| 0 | $d_0 = 4\left(\frac{\Delta^2}{\gamma^2} - p^2\right)^3$ | $K = \sqrt[3]{\frac{c_3}{6} + \sqrt{\frac{d_6}{108}}}$ |
| $c_1 = 4\left(\frac{\Delta}{\gamma}\right)^2 + 2p^2$ | $d_1 = -48p^2\left(\frac{\Delta^2}{\gamma^2} - p^2\right)^2$ | $b_1 = \frac{\frac{c_2}{6} + \sqrt{\frac{d_6}{108}} u_1}{\sqrt[3]{\frac{c_3}{6} + \sqrt{\frac{d_6}{108}}}}$ |
| $c_2 = 8p^2$ | $d_2 = 12\left(2\frac{\Delta^2}{\gamma^2} + p^2\right)^2 + 192p^4\left(\frac{\Delta^2}{\gamma^2} - p^2\right) - 4(4 + 9p^2)\left(\frac{\Delta^2}{\gamma^2} - p^2\right)^2$ | $b_2 = \frac{\frac{c_1}{6} + \sqrt{\frac{d_6}{108}} u_2}{\sqrt[3]{\frac{c_3}{6} + \sqrt{\frac{d_6}{108}}}}$ |
| $c_3 = \frac{(16+54p^2)}{9}$ | $d_3 = 96p^2\left(2\frac{\Delta^2}{\gamma^2} + p^2\right) + 32p^2(4 + 9p^2)\left(\frac{\Delta^2}{\gamma^2} - p^2\right) - 256p^6$ | $b_3 = \frac{\sqrt{\frac{d_6}{108}} u_3}{\sqrt[3]{\frac{c_3}{6} + \sqrt{\frac{d_6}{108}}}}$ |
| 0 | $d_4 = \frac{8}{3}(8 + 27p^2)\left(2\frac{\Delta^2}{\gamma^2} + p^2\right) + \frac{4}{3}(4 + 9p^2)^2\left(\frac{\Delta^2}{\gamma^2} - p^2\right) - 64p^4(1 + 9p^2)$ | $b_4 = \frac{\sqrt{\frac{d_6}{108}} u_4}{\sqrt[3]{\frac{c_3}{6} + \sqrt{\frac{d_6}{108}}}}$ |
| 0 | $d_5 = -16p^4(6 + 27p^2)$ | $b_5 = \frac{\sqrt{\frac{d_6}{108}} u_5}{\sqrt[3]{\frac{c_3}{6} + \sqrt{\frac{d_6}{108}}}}$ |
| 0 | $d_6 = -36p^4(1 + 3p^2)$ | $b_6 = \frac{\sqrt{\frac{d_6}{108}} u_6}{\sqrt[3]{\frac{c_3}{6} + \sqrt{\frac{d_6}{108}}}}$ |

TABLE II. The expansion coefficients u_k and v_k in the expressions for \sqrt{D} and $\Lambda(x)$.

| u_i | v_i |
|--|---|
| $u_1 = \frac{1}{2} \frac{d_5}{d_6}$ | $v_1 = \frac{b_1}{3}$ |
| $u_2 = \frac{1}{2} \frac{d_4}{d_6} - \frac{1}{8} \left(\frac{d_5}{d_6}\right)^2$ | $v_2 = \frac{b_2}{3} - \frac{b_1^2}{9}$ |
| $u_3 = \frac{1}{2} \frac{d_3}{d_6} - \frac{1}{8} 2 \frac{d_4 d_5}{d_6^2} + \frac{3}{48} \left(\frac{d_5}{d_6}\right)^3$ | $v_3 = \frac{b_3}{3} - \frac{2b_1 b_2}{9} + \frac{5b_1^3}{81}$ |
| $u_4 = \frac{1}{2} \frac{d_2}{d_6} - \frac{1}{8} \left[2 \frac{d_3 d_5}{d_6^2} + \left(\frac{d_4}{d_6}\right)^2 \right] + \frac{3}{48} \left(3 \frac{d_4 d_5^2}{d_6^3} \right) - \frac{15}{384} \left(\frac{d_5}{d_6}\right)^4$ | $v_4 = \frac{b_4}{3} - \frac{(2b_1 b_3 + b_2^2)}{9} + \frac{5(3b_1^2 b_2)}{81}$ |
| $u_5 = \frac{1}{2} \frac{d_1}{d_6} - \frac{1}{8} \left(2 \frac{d_2 d_5}{d_6^2} + 2 \frac{d_3 d_4}{d_6^2} \right) + \frac{3}{48} \left(3 \frac{d_3 d_5^2}{d_6^3} + 3 \frac{d_4^2 d_5}{d_6^3} \right) - \frac{15}{384} \left(4 \frac{d_4 d_5^3}{d_6^4} \right)$ | $v_5 = \frac{b_5}{3} - \frac{(2b_1 b_4 + 2b_2 b_3)}{9} + \frac{5(3b_1^2 b_3 + 3b_1 b_2^2)}{81}$ |
| $u_6 = \frac{1}{2} \frac{d_0}{d_6} - \frac{1}{8} \left[2 \frac{d_1 d_5}{d_6^2} + 2 \frac{d_2 d_4}{d_6^2} + \left(\frac{d_3}{d_6}\right)^3 \right] + \frac{3}{48} \left[3 \frac{d_2 d_5^2}{d_6^3} + 6 \frac{d_3 d_4 d_5}{d_6^3} + \left(\frac{d_4}{d_6}\right)^3 \right] - \frac{15}{384} \left(4 \frac{d_3 d_5^3}{d_6^4} + 6 \frac{d_4^2 d_5^2}{d_6^4} \right)$ | $v_6 = \frac{b_6}{3} - \frac{(2b_1 b_5 + 2b_2 b_4 + b_3^2)}{9} + \frac{5(3b_1^2 b_4 + 6b_1 b_2 b_3 + b_2^3)}{81}$ |

Substituting Eqs. (A6) and (A8) into Eq. (A1) we obtain the general expression of the discriminant as the polynomial function of the occupation number (i.e., $\bar{n} = \frac{r}{\gamma}$),

$$D = \frac{\gamma^6}{108} \sum_{k=0}^6 d_k \bar{n}^k, \tag{A9}$$

where the expansion coefficients d_k are listed in Table I.

For large $\frac{\Delta}{\gamma}$ and \bar{n} , the significant terms in Eq. (9) are the sixth order terms d_0 , $d_4 \bar{n}^4$, and $d_6 \bar{n}^6$,

$$D = \frac{\gamma^6}{108} (d_0 + d_4 \bar{n}^4 + d_6 \bar{n}^6). \tag{A10}$$

To solve the equation $D = 0$, we take $\frac{\Delta}{\gamma} = y$, $\bar{n} = x$ and simplify as

$$\begin{aligned} & 4(y^2 - p^2)^3 + \left[\frac{8}{3}(8 + 27p^2)(2y^2 + p^2) \right. \\ & \quad \left. + \frac{4}{3}(4 + 9p^2)^2(y^2 - p^2) - 64p^4(1 + 9p^2) \right] x^4 \\ & \quad - 36p^4(1 + 3p^2)x^6 = 0, \\ & 4y^6 + \left[\frac{8}{3}(8 + 27p^2)2y^2 + \frac{4}{3}(4 + 9p^2)^2 y^2 \right. \\ & \quad \left. - 64p^4(1 + 9p^2) \right] x^4 - 36p^4(1 + 3p^2)x^6 = 0. \end{aligned}$$

TABLE III. The expansion coefficients \mathcal{W}_k and z_{jk} in the expression of $\frac{1}{T}$ in Eq. (A40) and λ_j in Eq. (A43).

| \mathcal{W}_i | z_{ji} |
|--|---|
| 0 | $z_{j0} = -\frac{5}{3} - \frac{\alpha_j}{3K} \left(\frac{4}{3} + 3p^2 \right) - \beta_j K$ |
| $\mathcal{W}_1 = -v_1$ | $z_{j1} = -1 - \frac{\alpha_j}{3K} \left[4p^2 + \left(\frac{4}{3} + 3p^2 \right) W_1 \right] - \beta_j K v_1$ |
| $\mathcal{W}_2 = -v_2 + v_1^2$ | $z_{j2} = \frac{\alpha_j}{3K} \left[\left(\frac{\Delta^2}{\gamma^2} - p^2 \right) - 4p^2 W_1 - \left(\frac{4}{3} + 3p^2 \right) W_2 \right] - \beta_j K v_2$ |
| $\mathcal{W}_3 = -v_3 + 2v_1 v_2 - v_1^3$ | $z_{j3} = \frac{\alpha_j}{3K} \left[\left(\frac{\Delta^2}{\gamma^2} - p^2 \right) W_1 - 4p^2 W_2 - \left(\frac{4}{3} + 3p^2 \right) W_3 \right] - \beta_j K v_3$ |
| $\mathcal{W}_4 = -v_4 + (2v_1 v_3 + v_2^2) - 3v_1^2 v_2 + v_1^4$ | $z_{j4} = \frac{\alpha_j}{3K} \left[\left(\frac{\Delta^2}{\gamma^2} - p^2 \right) W_2 - 4p^2 W_3 - \left(\frac{4}{3} + 3p^2 \right) W_4 \right] - \beta_j K v_4$ |
| $\mathcal{W}_5 = -v_5 + (2v_1 v_4 + 2v_2 v_3) - (3v_1^2 v_3 + 3v_1 v_2^2) + 4v_1^3 v_2 - v_1^5$ | $z_{j5} = \frac{\alpha_j}{3K} \left[\left(\frac{\Delta^2}{\gamma^2} - p^2 \right) W_3 - 4p^2 W_4 - \left(\frac{4}{3} + 3p^2 \right) W_5 \right] - \beta_j K v_5$ |
| $\mathcal{W}_6 = -v_6 + (2v_1 v_5 + 2v_2 v_4 + v_3^2) - (3v_1^2 v_4 + 6v_1 v_2 v_3 + v_2^3) + (4v_1^3 v_3 + 6v_1^2 v_2^2) + v_1^6$ | $z_{j6} = \frac{\alpha_j}{3K} \left[\left(\frac{\Delta^2}{\gamma^2} - p^2 \right) W_4 - 4p^2 W_5 - \left(\frac{4}{3} + 3p^2 \right) W_6 \right] - \beta_j K v_6$ |
| 0 | $z_{j7} = \frac{\alpha_j}{3K} \left[\left(\frac{\Delta^2}{\gamma^2} - p^2 \right) W_5 - 4p^2 W_6 \right]$ |
| 0 | $z_{j8} = \frac{\alpha_j}{3K} \left[\left(\frac{\Delta^2}{\gamma^2} - p^2 \right) W_6 \right]$ |

Dividing on both sides by x^6 , we get

$$\begin{aligned} & 4\left(\frac{y}{x}\right)^6 + \left[\frac{16}{3}(8 + 27p^2) + \frac{4}{3}(4 + 9p^2)^2 \right] \left(\frac{y}{x}\right)^2 \\ & \quad - 64p^4(1 + 9p^2) \frac{1}{x^2} - 36p^4(1 + 3p^2) = 0. \end{aligned}$$

Neglecting the term proportional to $\frac{1}{x^2}$ for large $\bar{n} = x$ and defining $\left(\frac{y}{x}\right)^2 = z$, the above equation reduces to the form of a depressed cubic

$$z^3 + Pz + Q = 0, \tag{A11}$$

where

$$P = (16 + 60p^2 + 27p^4), \tag{A12}$$

$$Q = -9p^4(1 + 3p^2). \tag{A13}$$

To solve the depressed cubic equation, we substitute $z = u + v$ into Eq. (11) which becomes

$$u^3 + v^3 + (u + v)(3uv + P) + Q = 0. \tag{A14}$$

The arbitrary variables u, v are chosen in such a way that

$$(3uv + P) = 0, \quad uv = -\frac{P}{3}. \tag{A15}$$

TABLE IV. Coefficients z_{j2} and v_2 .

| z_{j2} | v_2 |
|--|---|
| $f_{j1}(p) = \frac{\alpha_j}{3K} + \left[\frac{\alpha_j}{3K} \left(\frac{4}{3} + 3p^2 \right) - \beta_j K \right] s_1(p)$ | $s_1(p) = \frac{l_1(p)}{3}$ |
| $f_{j2}(p) = -\frac{\alpha_j}{3K} p^2 + 4p^2 \left(\frac{\alpha_j}{3K} \right) v_1 + \left[\frac{\alpha_j}{3K} \left(\frac{4}{3} + 3p^2 \right) - \beta_j K \right] s_2(p) - \frac{\alpha_j}{3K} \left(\frac{4}{3} + 3p^2 \right) v_1^2$ | $s_2(p) = \frac{l_2(p)}{3} - \left[\frac{1}{3K} \left(\frac{4p^2}{3} + \frac{2}{9} \frac{p^2(6+27p^2)}{(1+3p^2)} \sqrt{\frac{(1+3p^2)}{3}} i \right) \right]^2$ |

Cubing Eq. (A15) on both sides and expressing v^3 in terms of u^3 , we get

$$v^3 = -\frac{P^3}{27} \frac{1}{u^3}. \quad (\text{A16})$$

Using Eqs. (A15) and (A16) into Eq. (A14), we rearrange terms to get a quadratic equation in $u^3 = t$,

$$t^2 + Qt - \frac{4P^3}{27} = 0. \quad (\text{A17})$$

The two roots of the above equation are

$$t_1 = -\frac{Q}{2} + \sqrt{\frac{Q^2}{4} + \frac{P^3}{27}}, \quad (\text{A18})$$

$$t_2 = -\frac{Q}{2} - \sqrt{\frac{Q^2}{4} + \frac{P^3}{27}}. \quad (\text{A19})$$

We set $u^3 = t_1$, $v^3 = t_2$ which satisfy the required conditions $u^3 + v^3 = -Q$, $u^3 v^3 = -\frac{P^3}{27}$. This shows that $u = \sqrt[3]{t_1}$ and $v = \sqrt[3]{t_2}$ are solutions to Eq. (A14). As $z = \left(\frac{y}{x}\right)^2$ cannot be complex valued and $\sqrt[3]{t_1}$, $\sqrt[3]{t_2}$ are real and positive for all p values, the real solution for z is

$$\begin{aligned} z &= u + v, \\ \left(\frac{y}{x}\right)^2 &= \sqrt[3]{t_1} + \sqrt[3]{t_2}, \\ \frac{\Delta}{\gamma} &= \sqrt{\sqrt[3]{t_1} + \sqrt[3]{t_2}} \bar{n}, \\ \frac{\Delta}{\gamma} &= f(p) \bar{n}, \end{aligned} \quad (\text{A20})$$

where

$$f(p) = \sqrt{\sqrt[3]{t_1} + \sqrt[3]{t_2}}, \quad (\text{A21})$$

with t_1 and t_2 given by Eqs. (A18) and (A19). This shows that in the strong pumping limit and when $\frac{\Delta}{\gamma}$ and \bar{n} are large, the critical $D = 0$ line behaves as a straight line with slope given by $m = f(p)$, a function of p only. A plot of $f(p)$ is shown in Fig. 4(a) of the main text.

2. Eigenvalues of matrix A

The eigenvalues λ_k of the coefficient matrix **A** are given by Cardano's solution of the characteristic equation

$$\lambda_j = -A + \alpha_j \frac{B}{\mathcal{T}} - \beta_j \mathcal{T} \quad (j = 1 - 3), \quad (\text{A22})$$

where

$$\mathcal{T} = \sqrt[3]{E + \sqrt{D}}, \quad (\text{A23})$$

$$E = \left[C - \frac{3}{2} A(B + A^2) \right], \quad (\text{A24})$$

$$D = B^3 + \left[C - \frac{3}{2} A(B + A^2) \right]^2, \quad (\text{A25})$$

$$\omega = \frac{-1 + i\sqrt{3}}{2}, \quad (\text{A26})$$

$$\omega^2 = \frac{-1 - i\sqrt{3}}{2}, \quad (\text{A27})$$

and $(\alpha_1, \beta_1) = (1, 1)$, $(\alpha_2, \beta_2) = (\omega^2, \omega)$, $(\alpha_3, \beta_3) = (\omega, \omega^2)$.

In the strong pumping limit where $\bar{n} \gg 1$, we define a new variable $x = 1/\bar{n} \ll 1$ and express the terms \mathcal{D} and E in the polynomial form of $x = 1/\bar{n} = \gamma/r$. We find the expression for E by rearranging Eq. (A8) as

$$E = \frac{r^3}{6} \sum_{k=1}^3 c_k x^{3-k}, \quad (\text{A28})$$

where the p -dependent expansion coefficients c_k ($k = 1, 2, 3$) are listed in Table I.

In order to simplify the term \mathcal{T} in the eigenvalue expression, we first express \sqrt{D} [with D given by Eq. (A9)] in the following form:

$$\sqrt{D} = r^3 \sqrt{\frac{d_6}{108}} \sqrt{[1 + \alpha(x)]}, \quad (\text{A29})$$

where

$$\alpha(x) = \frac{1}{d_6} \sum_{k=1}^6 d_{6-k} x^k. \quad (\text{A30})$$

TABLE V. Coefficients d_4 , u_2 , and b_2 in the expansion of z_{j2} .

| b_2 | u_2 | d_4 |
|--|---|----------------------------------|
| $l_1(p) = \frac{2}{3K} + \frac{p^2}{K} \sqrt{\frac{(1+3p^2)}{3}} g_1(p) i$ | $g_1(p) = -\frac{h_1(p)}{72p^4(1+3p^2)}$ | $h_1(p) = 4(16 + 60p^2 + 27p^4)$ |
| $l_2(p) = \frac{p^2}{3K} + \frac{p^2}{K} \sqrt{\frac{(1+3p^2)}{3}} g_2(p) i$ | $g_2(p) = -\frac{h_2(p)}{72p^4(1+3p^2)} - \frac{2}{81} \left(\frac{6+27p^2}{1+3p^2} \right)^2$ | $h_2(p) = -4p^4(22 + 171p^2)$ |

TABLE VI. Coefficients for the eigenvectors V_j , $j = 1, 2$ in Eq. (A44).

| $L_{jk}, j = 1, 2, 3$ | $k_{jk}, j = 1, 2$ | $a_{jk}, j = 1, 2$ | $b_{jk}, j = 1, 2$ |
|---|--|----------------------------|---|
| $L_{j0} = z_{j0}^2 + 4z_{j0} + 3(1 - p^2)$ | 0 | $a_{j0} = 1$ | $b_{j0} = 3 + z_{j0}$ |
| $L_{j1} = 2z_{j0}z_{j1} + 2z_{j0} + 4z_{j1} + 4(1 - p^2)$ | $k_{j1} = -\frac{L_{j3}}{L_{j2}}$ | $a_{j1} = 1 + k_{j1}$ | $b_{j1} = (1 + z_{j1}) + (3 + z_{j0})k_{j1}$ |
| $L_{j2} = z_{j1}^2 + 2z_{j0}z_{j2} + 2z_{j1} + 4z_{j2} + (1 - p^2)$ | $k_{j2} = -\frac{L_{j4}}{L_{j2}} + \left(\frac{L_{j3}}{L_{j2}}\right)^2$ | $a_{j2} = k_{j1} + k_{j2}$ | $b_{j2} = (1 + z_{j1})k_{j1} + (3 + z_{j0})k_{j2} + z_{j2}$ |
| $L_{j3} = 2z_{j1}z_{j2} + 2z_{j2}$ | $k_{j3} = \frac{2L_{j3}L_{j4}}{L_{j2}^2} - \left(\frac{L_{j3}}{L_{j2}}\right)^3$ | $a_{j3} = k_{j2} + k_{j3}$ | $b_{j3} = (1 + z_{j1})k_{j2} + (3 + z_{j0})k_{j3} + z_{j2}k_{j1}$ |
| $L_{j4} = z_{j2}^2$ | $k_{j4} = \left(\frac{L_{j4}}{L_{j2}}\right)^2 - \frac{3L_{j3}^2L_{j4}}{L_{j2}^3}$ | $a_{j4} = k_{j3} + k_{j4}$ | $b_{j4} = (1 + z_{j1})k_{j3} + (3 + z_{j0})k_{j4} + z_{j2}k_{j2}$ |
| 0 | $k_{j5} = -\frac{3L_{j3}L_{j4}^2}{L_{j2}^3}$ | $a_{j5} = k_{j4} + k_{j5}$ | $b_{j5} = (1 + z_{j1})k_{j4} + (3 + z_{j0})k_{j5} + z_{j2}k_{j3}$ |
| 0 | $k_{j6} = -\left(\frac{L_{j4}}{L_{j2}}\right)^2$ | $a_{j6} = k_{j5} + k_{j6}$ | $b_{j6} = (1 + z_{j1})k_{j5} + (3 + z_{j0})k_{j6} + z_{j2}k_{j4}$ |
| 0 | 0 | $a_{j7} = k_{j6}$ | $b_{j7} = (1 + z_{j1})k_{j6} + z_{j2}k_{j5}$ |
| 0 | 0 | 0 | $b_{j8} = z_{j2}k_{j6}$ |

In the strong pumping limit ($x = 1/\bar{n} \ll 1$) the terms $\frac{d_6-k}{d_6} x^k$, $k \geq 1$ are all negligible compared to 1 and thus $|\alpha(x)| \ll 1$. The binomial expansion presented here and all the succeeding expansions are valid for $\bar{n} \geq 10^2$ and $p > 0.1$ (for $\Delta/\gamma < 1$) and $0.89 < p < 1$ (for $\Delta/\gamma > 1$). Taking the binomial expansion of $\sqrt{1 + \alpha(x)}$,

$$(1 + \alpha)^{1/2} = 1 + \frac{1}{2}\alpha - \frac{1}{8}\alpha^2 + \frac{3}{48}\alpha^3 - \frac{15}{384}\alpha^4 + \frac{105}{3840}\alpha^5 - \dots, \tag{A31}$$

we find the terms α^k with $k \leq 4$ by using a multinomial expansion

$$\begin{aligned} \alpha^2 &= \left(\frac{d_5}{d_6}\right)^2 x^2 + \left(2\frac{d_4d_5}{d_6^2}\right)x^3 + \left[2\frac{d_3d_5}{d_6^2} + \left(\frac{d_4}{d_6}\right)^2\right]x^4 + \left(2\frac{d_2d_5}{d_6^2} + 2\frac{d_3d_4}{d_6^2}\right)x^5 + \left[2\frac{d_1d_5}{d_6^2} + 2\frac{d_2d_4}{d_6^2} + \left(\frac{d_4}{d_6}\right)^3\right]x^6, \\ \alpha^3 &= \left(\frac{d_5}{d_6}\right)^3 x^3 + \left(3\frac{d_4d_5^2}{d_6^3}\right)x^4 + \left(3\frac{d_3d_5^2}{d_6^3} + 3\frac{d_4^2d_5}{d_6^3}\right)x^5 + \left[3\frac{d_2d_5^2}{d_6^3} + 6\frac{d_3d_4d_5}{d_6^3} + \left(\frac{d_4}{d_6}\right)^3\right]x^6, \\ \alpha^4 &= \left(\frac{d_5}{d_6}\right)^4 x^4 + \left(4\frac{d_4d_5^3}{d_6^4}\right)x^5 + \left(4\frac{d_3d_5^3}{d_6^4} + 6\frac{d_4^2d_5^2}{d_6^4}\right)x^6. \end{aligned}$$

Substituting Eq. (A30) and the above expressions into Eq. (A29) we get

$$\sqrt{D} = r^3 \sqrt{\frac{d_6}{108}} \left[1 + \sum_{k=1}^6 u_k x^k \right], \tag{A32}$$

TABLE VII. Coefficients for the eigenvector V_j , $j = 3$ in Eq. (A44).

| $k_{jk}, j = 3$ | $a_{jk}, j = 3$ | $b_{jk}, j = 3$ |
|--|----------------------------|---|
| 0 | $a_{30} = 1$ | $b_{30} = 3 + z_{30}$ |
| $k_{31} = -\frac{L_{31}}{L_{30}}$ | $a_{31} = 1 + k_{31}$ | $b_{31} = (1 + z_{31}) + (3 + z_{30})k_{31}$ |
| $k_{32} = -\frac{L_{32}}{L_{30}} + \left(\frac{L_{31}}{L_{30}}\right)^2$ | $a_{32} = k_{31} + k_{32}$ | $b_{32} = (1 + z_{31})k_{31} + (3 + z_{30})k_{32} + z_{32}$ |
| $k_{33} = -\frac{L_{33}}{L_{30}} + \frac{2L_{31}L_{32}}{L_{30}^2} - \left(\frac{L_{31}}{L_{30}}\right)^3$ | $a_{33} = k_{32} + k_{33}$ | $b_{33} = (1 + z_{31})k_{32} + (3 + z_{30})k_{33} + z_{32}k_{31}$ |
| $k_{34} = -\frac{L_{34}}{L_{30}} + \left[\frac{2L_{31}L_{33}}{L_{30}^2} + \left(\frac{L_{32}}{L_{30}}\right)^2\right] - \left(\frac{3L_{31}^2L_{32}}{L_{30}^3} + \frac{3L_{31}L_{32}^2}{L_{30}^3}\right) + \left(\frac{L_{31}}{L_{30}}\right)^4$ | $a_{34} = k_{33} + k_{34}$ | $b_{34} = (1 + z_{31})k_{33} + (3 + z_{30})k_{34} + z_{32}k_{32}$ |
| $k_{35} = \left(\frac{2L_{31}L_{34}}{L_{30}^2} + \frac{2L_{32}L_{33}}{L_{30}^2}\right) - \frac{3L_{31}^2L_{33}}{L_{30}^3} + \left(\frac{4L_{31}^3L_{32}}{L_{30}^3} - \left(\frac{L_{31}}{L_{30}}\right)^5\right)$ | $a_{35} = k_{34} + k_{35}$ | $b_{35} = (1 + z_{31})k_{34} + (3 + z_{30})k_{35} + z_{32}k_{33}$ |

TABLE VIII. Coefficients for L_{j2} , $j = 1, 2$ and the determinant of the eigenvector matrix \mathbf{M} .

| L_{j2} , $j = 1, 2$ | $\det(\mathbf{M})$ |
|--|---|
| $F_{j1}(p) = [4 + 2z_{j0}(p)]f_{j1}(p)$ | $T_1(p) = p\left(-\frac{m_1}{F_{11}} - \frac{m_5}{F_{21}}\right)$ |
| $F_{j2}(p) = [4 + 2z_{j0}(p)]f_{j2}(p) + [z_{j1}(p)^2 + 2z_{j1}(p) + (1 - p^2)]$ | $T_2(p) = p\left(-\frac{m_2}{F_{11}} + \frac{f_{11}}{F_{11}} \frac{1}{(2z_{10}+4)} - \frac{m_6}{F_{21}} - \frac{m_{11}}{L_{30}}\right)$ |

where the expansion coefficients u_k are listed in Table II. Now, using Eqs. (A28) and (A32) in Eq. (A23) the term \mathcal{T} can be expanded as

$$\begin{aligned} \mathcal{T} &= \left[\frac{r^3}{6} \sum_{k=1}^3 c_k x^{3-k} + r^3 \sqrt{\frac{d_6}{108}} \left(1 + \sum_{k=1}^6 u_k x^k \right) \right]^{1/3} \\ &= r \sqrt[3]{\frac{c_3}{6} + \sqrt{\frac{d_6}{108}}} \left[1 + \frac{\sum_{k=1}^2 \left(\frac{c_{3-k}}{6} + \sqrt{\frac{d_6}{108}} u_k \right)}{\sqrt[3]{\frac{c_3}{6} + \sqrt{\frac{d_6}{108}}}} x^k + \frac{\sum_{k=3}^6 \sqrt{\frac{d_6}{108}} u_k}{\sqrt[3]{\frac{c_3}{6} + \sqrt{\frac{d_6}{108}}}} x^k \right]^{1/3} \\ &= rK \left[1 + \sum_{k=1}^6 b_k x^k \right]^{1/3}, \end{aligned} \tag{A33}$$

where the term K and the coefficients b_k are listed in Table I. Equation (A33) can be rewritten as

$$\mathcal{T} = rK[1 + \beta(x)]^{1/3}, \tag{A34}$$

where

$$\beta(x) = \sum_{k=1}^6 b_k x^k.$$

In the strong pumping limit ($x = 1/\bar{n} \ll 1$), the terms $b_k x^k$, $k \geq 1$ are all negligible compared to 1 and thus $|\beta(x)| \ll 1$. Taking the binomial expansion of $\sqrt[3]{1 + \beta}$,

$$(1 + \beta)^{1/3} = 1 + \frac{1}{3}\beta - \frac{1}{9}\beta^2 + \frac{5}{81}\beta^3 - \frac{10}{243}\beta^4 + \dots, \tag{A35}$$

evaluating the terms β^k with $k \leq 3$ using the multinomial expansion

$$\begin{aligned} \beta^2 &= b_1^2 x^2 + 2b_1 b_2 x^3 + (2b_1 b_3 + b_2^2) x^4 + (2b_1 b_4 + 2b_2 b_3) x^5 + (2b_1 b_5 + 2b_2 b_4 + b_3^2) x^6 + \dots, \\ \beta^3 &= b_1^3 x^3 + (3b_1^2 b_2) x^4 + (3b_1^2 b_3 + 3b_1 b_2^2) x^5 + (3b_1^2 b_4 + 6b_1 b_2 b_3 + b_2^3) x^6 + \dots, \end{aligned}$$

and substituting the result in Eq. (A34), we get

$$\mathcal{T} = rK \left[1 + \sum_{k=1}^6 v_k x^k \right], \tag{A36}$$

where the expansion coefficients v_k are listed in Table II. The second term in the eigenvalue expression contains the fraction $\frac{1}{\mathcal{T}}$, which we simplify to obtain

$$\frac{1}{\mathcal{T}} = \frac{1}{rK} \left[1 + \sum_{k=1}^6 v_k x^k \right]^{-1} = \frac{1}{rK} [1 + \Lambda(x)]^{-1}, \tag{A37}$$

TABLE IX. Components V_{ij} , $i, j = 1, 2, 3$ of the eigenvector matrix \mathbf{M} in Eq. (A71).

| V_{1i} | V_{2i} | V_{3i} |
|---|--|--|
| $V_{11} = p \left[-\frac{1}{F_{11}} + \frac{f_{11}}{F_{11}} \frac{1}{(2z_{10}+4)} \frac{1}{\bar{n}^2} \left(\frac{\Delta}{\gamma} \right)^2 \right] \bar{n} \left(\frac{\Delta}{\gamma} \right)^{-1}$ | $V_{21} = -\frac{p}{F_{21}} \bar{n} \left(\frac{\Delta}{\gamma} \right)^{-1}$ | $V_{31} = -\frac{p}{L_{30}} \left(\frac{1}{\bar{n}} \right) \left(\frac{\Delta}{\gamma} \right)$ |
| $V_{12} = \left[\frac{(3+z_{10})}{F_{11}} + \left(\frac{f_{11}}{F_{11}} \right) \frac{(1+z_{10})}{(4+2z_{10})} \left(\frac{1}{\bar{n}} \right)^2 \left(\frac{\Delta}{\gamma} \right)^2 \right] \bar{n} \left(\frac{\Delta}{\gamma} \right)^{-1}$ | $V_{22} = \frac{(3+z_{20})}{F_{21}} \bar{n} \left(\frac{\Delta}{\gamma} \right)^{-1}$ | $V_{32} = \frac{(3+z_{30})}{L_{30}} \left(\frac{1}{\bar{n}} \right) \left(\frac{\Delta}{\gamma} \right)$ |
| $V_{13} = 1$ | $V_{23} = 1$ | $V_{33} = 1$ |

TABLE X. Cofactors T_{ij} , $i, j = 1, 2, 3$ of the eigenvector matrix \mathbf{M} in Eq. (A71).

| T_{1i} | T_{2i} | T_{3i} |
|---|---|---|
| $T_{11} = [m_1(p) + m_2(p)\frac{1}{\bar{n}^2}(\frac{\Delta}{\gamma})^2]\bar{n}(\frac{\Delta}{\gamma})^{-1}$ | $T_{21} = [m_5(p) + m_6(p)\frac{1}{\bar{n}^2}(\frac{\Delta}{\gamma})^2]\bar{n}(\frac{\Delta}{\gamma})^{-1}$ | $T_{31} = [m_{11}(p) + m_{12}(p)\frac{1}{\bar{n}^2}(\frac{\Delta}{\gamma})^2]\bar{n}(\frac{\Delta}{\gamma})^{-1}$ |
| $T_{12} = [m_3(p) + m_4(p)\frac{1}{\bar{n}^2}(\frac{\Delta}{\gamma})^2]\bar{n}(\frac{\Delta}{\gamma})^{-1}$ | $T_{22} = [m_7(p) + m_8(p)\frac{1}{\bar{n}^2}(\frac{\Delta}{\gamma})^2]\bar{n}(\frac{\Delta}{\gamma})^{-1}$ | $T_{32} = [m_{13}(p) + m_{14}(p)\frac{1}{\bar{n}^2}(\frac{\Delta}{\gamma})^2]\bar{n}(\frac{\Delta}{\gamma})^{-1}$ |
| $T_{13} = \frac{p}{F_{21}L_{30}}(z_{20} - z_{30})$ | $T_{23} = [m_9(p) + m_{10}(p)\frac{1}{\bar{n}^2}(\frac{\Delta}{\gamma})^2]$ | $T_{33} = [m_{15}(p) + m_{16}(p)\frac{1}{\bar{n}^2}(\frac{\Delta}{\gamma})^2]\bar{n}^2(\frac{\Delta}{\gamma})^{-2}$ |

where

$$\Lambda(x) = \sum_{k=1}^6 v_k x^k. \tag{A38}$$

In the strong pumping limit ($x = 1/\bar{n} \ll 1$) the terms $v_k x^k$, $k \geq 1$ are all negligible compared to 1 and thus $|\Lambda(x)| \ll 1$. Taking the binomial expansion of $(1 + \Lambda)^{-1}$,

$$(1 + \Lambda)^{-1} = 1 - \Lambda + \Lambda^2 - \Lambda^3 + \Lambda^4 - \Lambda^5 + \dots, \tag{A39}$$

we find the terms Λ^k with $k \leq 4$ by using the multinomial expansion

$$\begin{aligned} \Lambda^2 &= v_1^2 x^2 + 2v_1 v_2 x^3 + (2v_1 v_3 + v_2^2) x^4 + (2v_1 v_4 + 2v_2 v_3) x^5 + (2v_1 v_5 + 2v_2 v_4 + v_3^2) x^6, \\ \Lambda^3 &= v_1^3 x^3 + 3v_1^2 v_2 x^4 + (3v_1^2 v_3 + 3v_1 v_2^2) x^5 + (3v_1^2 v_4 + 6v_1 v_2 v_3 + v_2^3) x^6, \\ \Lambda^4 &= v_1^4 x^4 + 4v_1^3 v_2 x^5 + (4v_1^3 v_3 + 6v_1^2 v_2^2) x^6. \end{aligned}$$

Substituting the above expressions into Eq. (A37), we obtain

$$\frac{1}{\mathcal{T}} = \frac{1}{rK} \left[1 + \sum_{k=1}^6 \mathcal{W}_k x^k \right], \tag{A40}$$

where the expansion coefficients \mathcal{W}_k are listed in Table III. Now we evaluate the second term $\frac{B}{\mathcal{T}}$ of the eigenvalue expression given by Eq. (A22). In the polynomial form of $x = 1/\bar{n}$, we have

$$B = \frac{r^2}{3} \left[\left(\frac{\Delta^2}{\gamma^2} - p^2 \right) x^2 - 4p^2 x - \left(\frac{4}{3} + 3p^2 \right) \right]. \tag{A41}$$

Multiplying Eqs. (A40) and (A41) we get

$$\begin{aligned} \frac{B}{\mathcal{T}} &= \frac{r^2}{3} \left[\left(\frac{\Delta^2}{\gamma^2} - p^2 \right) x^2 - 4p^2 x - \left(\frac{4}{3} + 3p^2 \right) \right] \frac{1}{rK} \left[1 + \sum_{k=1}^6 \mathcal{W}_k x^k \right] \\ &= \frac{r}{3K} \left\{ - \left(\frac{4}{3} + 3p^2 \right) - \left[\left(\frac{4}{3} + 3p^2 \right) \mathcal{W}_1 + 4p^2 \right] x + \left[\left(\frac{\Delta^2}{\gamma^2} - p^2 \right) - 4p^2 \mathcal{W}_1 - \left(\frac{4}{3} + 3p^2 \right) \mathcal{W}_2 \right] x^2 \right. \\ &\quad + \left[\left(\frac{\Delta^2}{\gamma^2} - p^2 \right) \mathcal{W}_1 - 4p^2 \mathcal{W}_2 - \left(\frac{4}{3} + 3p^2 \right) \mathcal{W}_3 \right] x^3 + \left[\left(\frac{\Delta^2}{\gamma^2} - p^2 \right) \mathcal{W}_2 - 4p^2 \mathcal{W}_3 - \left(\frac{4}{3} + 3p^2 \right) \mathcal{W}_4 \right] x^4 \\ &\quad + \left[\left(\frac{\Delta^2}{\gamma^2} - p^2 \right) \mathcal{W}_3 - 4p^2 \mathcal{W}_4 - \left(\frac{4}{3} + 3p^2 \right) \mathcal{W}_5 \right] x^5 + \left[\left(\frac{\Delta^2}{\gamma^2} - p^2 \right) \mathcal{W}_4 - 4p^2 \mathcal{W}_5 - \left(\frac{4}{3} + 3p^2 \right) \mathcal{W}_6 \right] x^6 \\ &\quad \left. + \left[\left(\frac{\Delta^2}{\gamma^2} - p^2 \right) \mathcal{W}_5 - 4p^2 \mathcal{W}_6 \right] x^7 + \left(\frac{\Delta^2}{\gamma^2} - p^2 \right) \mathcal{W}_6 x^8 \right\}. \tag{A42} \end{aligned}$$

TABLE XI. Coefficients $m_i(p)$ for the cofactors T_{ij} of the eigenvector matrix \mathbf{M} .

| | | | |
|---------------------------------------|---|---|---|
| $m_1(p) = \frac{(3+z_{20})}{F_{21}}$ | $m_5(p) = -\frac{(3+z_{10})}{F_{11}}$ | $m_9(p) = \frac{p}{F_{11}L_{30}}(z_{10} + z_{30} + 6)$ | $m_{13}(p) = p\left(\frac{1}{F_{11}} - \frac{1}{F_{21}}\right)$ |
| $m_2(p) = -\frac{(3+z_{30})}{F_{31}}$ | $m_6(p) = -\left(\frac{f_{11}}{F_{11}} \frac{(1+z_{10})}{(4+2z_{10})} - \frac{(3+z_{30})}{L_{30}}\right)$ | $m_{10}(p) = p\left(\frac{f_{11}}{F_{11}L_{30}} \frac{(z_{10}-z_{30}-2)}{(2z_{10}+4)}\right)$ | $m_{14}(p) = -\left(\frac{f_{11}}{F_{11}} \frac{1}{(2z_{10}+4)}\right)$ |
| $m_3(p) = \frac{p}{F_{21}}$ | $m_7(p) = -\frac{p}{F_{11}}$ | $m_{11}(p) = \left(\frac{(3+z_{10})}{F_{11}} - \frac{(3+z_{20})}{F_{21}}\right)$ | $m_{15}(p) = p\left(\frac{(z_{10}-z_{20})}{F_{11}F_{21}}\right)$ |
| $m_4(p) = -\frac{p}{L_{30}}$ | $m_8(p) = p\left(\frac{f_{11}}{F_{11}} \frac{1}{(2z_{10}+4)} + \frac{1}{L_{30}}\right)$ | $m_{12}(p) = \left(\frac{f_{11}}{F_{11}} \frac{(1+z_{10})}{(4+2z_{10})}\right)$ | $m_{16}(p) = p\left(\frac{f_{11}}{F_{11}F_{21}} \frac{(z_{10}+z_{20}+4)}{(2z_{10}+4)}\right)$ |

TABLE XII. Coefficients $A_i(p)$, $B_i(p)$, and $C_i(p)$ for the population and coherence terms in Eqs. (A99) to (A101).

| A_i | B_i | C_i |
|---|---|----------------------------|
| $A_1 = -\frac{p}{F_{11}}(m_1 + pm_3)$ | $B_1 = \frac{(3+z_{10})}{F_{11}}(m_1 + pm_3)$ | $C_1 = (m_1 + pm_3)$ |
| $A_2 = p\left[\frac{f_{11}}{F_{11}}\frac{1}{(2z_{10}+4)}(m_1 + pm_3) - \frac{1}{F_{11}}(m_2 + pm_4)\right]$ | $B_2 = \left[\frac{f_{11}}{F_{11}}\frac{1}{(2z_{10}+4)}(m_1 + pm_3) + \frac{(3+z_{10})}{F_{11}}(m_2 + pm_4)\right]$ | $C_2 = (m_2 + pm_4)$ |
| $A_3 = -\frac{p}{F_{21}}(m_5 + pm_7)$ | $B_3 = \frac{(3+z_{20})}{F_{21}}(m_5 + pm_7)$ | $C_3 = (m_5 + pm_7)$ |
| $A_4 = -\frac{p}{F_{21}}(m_6 + pm_8)$ | $B_4 = \frac{(3+z_{20})}{F_{21}}(m_6 + pm_8)$ | $C_4 = (m_6 + pm_8)$ |
| $A_5 = -\frac{p}{L_{30}}(m_{11} + pm_{13})$ | $B_5 = \frac{(3+z_{30})}{L_{30}}(m_{11} + pm_{13})$ | $C_5 = (m_{11} + pm_{13})$ |
| $A_6 = -\frac{p}{L_{30}}(m_{12} + pm_{14})$ | $B_6 = \frac{(3+z_{30})}{L_{30}}(m_{12} + pm_{14})$ | $C_6 = (m_{12} + pm_{14})$ |

Substituting the expressions of A , $\frac{B}{T}$, and \mathcal{T} in Eq. (A22) and simplifying, we get Eq. (9) of the main text for the eigenvalues of the coefficient matrix

$$\lambda_j = r \sum_{k=0}^8 z_{jk} x^k \quad (j = 1-3), \quad (\text{A43})$$

where the expansion coefficients z_{jk} are listed in Table III.

3. Eigenvectors of matrix \mathbf{A}

The general expression for the eigenvectors of the coefficient matrix \mathbf{A} is obtained by solving the system of linear equations $(\mathbf{A} - \lambda_j)V_j = 0$ to yield

$$V_j = \begin{bmatrix} \frac{\Delta p(r+\gamma)}{\mathcal{D}_j} \\ -\frac{\Delta(3r+\gamma+\lambda_j)}{\mathcal{D}_j} \\ 1.0 \end{bmatrix} \quad (j = 1-3), \quad (\text{A44})$$

where

$$\mathcal{D}_j = -\lambda_j^2 - 2(\gamma + 2r)\lambda_j - (1 - p^2)\gamma^2 - 4\gamma r(1 - p^2) + 3r^2(1 - p^2). \quad (\text{A45})$$

a. Eigenvectors in the overdamped regime $[\Delta/(\bar{n}\gamma) < f(p)]$

In the strong pumping regime ($x \ll 1$), the terms x^n with $n \geq 3$ in Eq. (A43) can be neglected and the eigenvalues are given by

$$\lambda_j = r[z_{j0} + z_{j1}x + z_{j2}x^2]. \quad (\text{A46})$$

To evaluate the term \mathcal{D}_j , we evaluate the square of λ_j as

$$\lambda_j^2 = r^2[z_{j0}^2 + 2z_{j0}z_{j1}x + (z_{j1}^2 + 2z_{j0}z_{j2})x^2 + 2z_{j1}z_{j2}x^3 + z_{j2}^2x^4]. \quad (\text{A47})$$

Substituting Eqs. (A46) and (A47) into Eq. (A45) we obtain

$$\mathcal{D}_j = -r^2 \sum_{k=0}^4 L_{jk} x^k, \quad (\text{A48})$$

where the expansion coefficients L_{jk} are listed in Table VI. For the first eigenvector \vec{V}_1 , we find

$$\mathcal{D}_1 = -r^2 \sum_{k=0}^4 L_{1k} x^k. \quad (\text{A49})$$

In particular, the terms L_{10} , $L_{11}x$ are negligible compared to other terms in Eq. (A49) and are dropped. To find $\frac{1}{\mathcal{D}_1}$ required to evaluate Eq. (A44), we proceed as follows:

$$\begin{aligned} \frac{1}{\mathcal{D}_1} &= -\frac{1}{r^2 L_{12} x^2 [1 + \frac{L_{13}}{L_{12}} x + \frac{L_{14}}{L_{12}} x^2]} \\ &= -\frac{1}{r^2 L_{12} x^2} [1 + \alpha(x)]^{-1}, \end{aligned} \quad (\text{A50})$$

where

$$\alpha(x) = \frac{L_{13}}{L_{12}} x + \frac{L_{14}}{L_{12}} x^2. \quad (\text{A51})$$

For $x \ll 1$, $\alpha(x) = (\frac{L_{13}}{L_{12}} x + \frac{L_{14}}{L_{12}} x^2) \ll 1$ and we can use the binomial expansion to get

$$(1 + \alpha)^{-1} = 1 - \alpha + \alpha^2 - \alpha^3 + \dots \quad (\text{A52})$$

Evaluating the terms up to the third order in α ,

$$\begin{aligned} \alpha^2 &= \left(\frac{L_{13}}{L_{12}}\right)^2 x^2 + \frac{2L_{13}L_{14}}{L_{12}^2} x^3 + \left(\frac{L_{14}}{L_{12}}\right)^2 x^4, \\ \alpha^3 &= \left(\frac{L_{13}}{L_{12}}\right)^3 x^3 + \frac{3L_{13}^2 L_{14}}{L_{12}^3} x^4 + \frac{3L_{13}L_{14}^2}{L_{12}^3} x^5 + \left(\frac{L_{14}}{L_{12}}\right)^3 x^6, \end{aligned} \quad (\text{A53})$$

and using Eqs. (A51) to (A54) in Eq. (A50) we get

$$\frac{1}{\mathcal{D}_1} = -\frac{1}{r^2 L_{12} x^2} \left[1 + \sum_{m=1}^6 k_{1m} x^m\right], \quad (\text{A55})$$

where the expansion coefficients k_{1m} are listed in Table VI.

We can now evaluate the first component of the eigenvector \vec{V}_1 as follows:

$$\begin{aligned} V_{11} &= \frac{\Delta p(\gamma + r)}{\mathcal{D}_1} \\ &= -\frac{p}{L_{12}} \frac{\Delta r(1 + \frac{\gamma}{r})}{r^2 (\frac{\gamma}{r})^2} \left[1 + \sum_{m=1}^6 k_{1m} x^m\right] \\ &= -\frac{p}{L_{12}} \left(\frac{\Delta}{\gamma}\right) \bar{n} \sum_{m=0}^7 a_{1m} x^m, \end{aligned} \quad (\text{A56})$$

where the expansion coefficients a_{1m} are listed in Table VI. Proceeding in a similar way, we find the second component of

the eigenvector \vec{V}_1 as

$$V_{12} = \frac{1}{L_{12}} \left(\frac{\Delta}{\gamma} \right) \bar{n} \sum_{m=0}^8 b_{1m} x^m, \quad (\text{A57})$$

where the expansion coefficients b_{1m} are listed in Table VI. The third component of the eigenvector \vec{V}_1 is $V_{13} = 1$.

Combining the expressions for V_{11} , V_{12} , and V_{13} , we obtain the first eigenvector as

$$\vec{V}_1 = \begin{bmatrix} -\frac{p}{L_{12}} \left(\frac{\Delta}{\gamma} \right) \bar{n} \sum_{m=0}^7 a_{1m} x^m \\ \frac{1}{L_{12}} \left(\frac{\Delta}{\gamma} \right) \bar{n} \sum_{m=0}^8 b_{1m} x^m \\ 1 \end{bmatrix}. \quad (\text{A58})$$

Proceeding in a similar way as for the first eigenvector \vec{V}_1 , we evaluate \mathcal{D}_2 and the components of the second eigenvector \vec{V}_2 ,

$$\vec{V}_2 = \begin{bmatrix} -\frac{p}{L_{22}} \left(\frac{\Delta}{\gamma} \right) \bar{n} \sum_{m=0}^7 a_{2m} x^m \\ \frac{1}{L_{22}} \left(\frac{\Delta}{\gamma} \right) \bar{n} \sum_{m=0}^8 b_{2m} x^m \\ 1 \end{bmatrix}, \quad (\text{A59})$$

where the coefficients L_{2k} , k_{2m} , a_{2m} , b_{2m} are listed in Table VI and z_{2k} ($k = 0-2$) are evaluated with $\alpha_2 = \omega^2$, $\beta_2 = \omega$.

For the third eigenvector \vec{V}_3 , the term \mathcal{D}_3 is given by

$$\mathcal{D}_3 = -r^2 \sum_{k=0}^4 L_{3k} x^k, \quad (\text{A60})$$

where the coefficients L_{3k} are listed in Table VI and z_{3k} ($k = 0-2$) are evaluated with $\alpha_3 = \omega$, $\beta_3 = \omega^2$.

Unlike in the case of the first and second eigenvectors, the terms L_{30} and $L_{31}x$ are not negligible compared to other $L_{3k}x^k$ terms. To find $\frac{1}{\mathcal{D}_3}$, we proceed as follows:

$$\begin{aligned} \frac{1}{\mathcal{D}_3} &= -\frac{1}{r^2 L_{30} \left[1 + \frac{1}{L_{30}} \sum_{k=1}^4 L_{3k} x^k \right]} \\ &= -\frac{1}{r^2 L_{30}} [1 + \alpha(x)]^{-1}, \end{aligned} \quad (\text{A61})$$

where

$$\alpha(x) = \frac{1}{L_{30}} \sum_{k=1}^4 L_{3k} x^k. \quad (\text{A62})$$

For $x \ll 1$, $\alpha(x) = \frac{1}{L_{30}} \sum_{k=1}^4 L_{3k} x^k \ll 1$. Taking the binomial expansion Eq. (A52) and evaluating the terms up to the fifth order in α and x we find

$$\begin{aligned} \alpha^2 &= \left(\frac{L_{31}^2}{L_{30}^2} \right) x^2 + \frac{2L_{31}L_{32}}{L_{30}^2} x^3 + \left(\frac{2L_{31}L_{33}}{L_{30}^2} + \frac{L_{32}^2}{L_{30}^2} \right) x^4 \\ &+ \left(\frac{2L_{31}L_{34}}{L_{30}^2} + \frac{2L_{32}L_{33}}{L_{30}^2} \right) x^5 + \dots, \end{aligned} \quad (\text{A63})$$

$$\begin{aligned} \alpha^3 &= \frac{L_{31}^3}{L_{30}^3} x^3 + \left(\frac{3L_{31}^2 L_{32}}{L_{30}^3} + \frac{3L_{31} L_{32}^2}{L_{30}^3} \right) x^4 \\ &+ \frac{3L_{31}^2 L_{33}}{L_{30}^3} x^5 + \dots, \end{aligned} \quad (\text{A64})$$

$$\alpha^4 = \frac{L_{31}^4}{L_{30}^4} x^4 + \frac{4L_{31}^3 L_{32}}{L_{30}^4} x^5 + \dots, \quad (\text{A65})$$

$$\alpha^5 = \frac{L_{31}^5}{L_{30}^5} x^5 + \dots. \quad (\text{A66})$$

Substituting Eqs. (A62) to (A66) into Eq. (A61) we get

$$\frac{1}{\mathcal{D}_3} = -\frac{1}{r^2 L_{30}} \left[1 + \sum_{m=1}^5 k_{3m} x^m \right], \quad (\text{A67})$$

where the expansion coefficients k_{3m} are listed in Table VII.

The first component of the eigenvector \vec{V}_3 is computed as

$$\begin{aligned} V_{31} &= \frac{\Delta p (\gamma + r)}{\mathcal{D}_3} \\ &= -\frac{p}{L_{30}} \frac{\Delta r (1+x)}{r^2} \left[1 + \sum_{m=1}^5 k_{3m} x^m \right] \\ &= -\frac{p}{L_{30}} \left(\frac{\Delta}{\gamma} \right) \frac{1}{\bar{n}} \sum_{m=0}^5 a_{3m} x^m, \end{aligned} \quad (\text{A68})$$

where the coefficients a_{3m} are listed in Table VII. Proceeding in the same way, the second component of the eigenvector \vec{V}_3 is evaluated as

$$V_{32} = \frac{1}{L_{30}} \left(\frac{\Delta}{\gamma} \right) \frac{1}{\bar{n}} \sum_{m=0}^8 b_{3m} x^m, \quad (\text{A69})$$

where the expansion coefficients b_{3m} are listed in Table VII. The third component of the eigenvector \vec{V}_3 is $V_{33} = 1$. The third eigenvector is thus

$$\vec{V}_3 = \begin{bmatrix} -\frac{p}{L_{30}} \left(\frac{\Delta}{\gamma} \right) \frac{1}{\bar{n}} \sum_{m=0}^5 a_{3m} x^m \\ \frac{1}{L_{30}} \left(\frac{\Delta}{\gamma} \right) \frac{1}{\bar{n}} \sum_{m=0}^8 b_{3m} x^m \\ 1 \end{bmatrix}. \quad (\text{A70})$$

Combining the expressions for the eigenvectors \vec{V}_1 , \vec{V}_2 , and \vec{V}_3 we obtain the matrix of eigenvectors of \mathbf{A} as

$$\mathbf{M} = \begin{bmatrix} -\frac{p}{L_{12}} \left(\frac{\Delta}{\gamma} \right) \bar{n} \sum_{m=0}^7 a_{1m} x^m & -\frac{p}{L_{22}} \left(\frac{\Delta}{\gamma} \right) \bar{n} \sum_{m=0}^7 a_{2m} x^m & -\frac{p}{L_{30}} \left(\frac{\Delta}{\gamma} \right) \frac{1}{\bar{n}} \sum_{m=0}^5 a_{3m} x^m \\ \frac{1}{L_{12}} \left(\frac{\Delta}{\gamma} \right) \bar{n} \sum_{m=0}^8 b_{1m} x^m & \frac{1}{L_{22}} \left(\frac{\Delta}{\gamma} \right) \bar{n} \sum_{m=0}^8 b_{2m} x^m & \frac{1}{L_{30}} \left(\frac{\Delta}{\gamma} \right) \frac{1}{\bar{n}} \sum_{m=0}^8 b_{3m} x^m \\ 1 & 1 & 1 \end{bmatrix}. \quad (\text{A71})$$

b. The determinant and the inverse of the eigenvector matrix \mathbf{M}

Expanding Eq. (A71) through second order in $x \ll 1$ and neglecting the insignificant terms, we get

$$\mathbf{M} = \begin{bmatrix} -\frac{p}{L_{12}}\left(\frac{\Delta}{\gamma}\right)\bar{n}(a_{10} + a_{12}x^2) & -\frac{p}{L_{22}}\left(\frac{\Delta}{\gamma}\right)\bar{n}a_{20} & -\frac{p}{L_{30}}\left(\frac{\Delta}{\gamma}\right)\left(\frac{1}{\bar{n}}\right)a_{30} \\ \frac{1}{L_{12}}\left(\frac{\Delta}{\gamma}\right)\bar{n}(b_{10} + b_{12}x^2) & \frac{1}{L_{22}}\left(\frac{\Delta}{\gamma}\right)\bar{n}b_{20} & \frac{1}{L_{30}}\left(\frac{\Delta}{\gamma}\right)\left(\frac{1}{\bar{n}}\right)b_{30} \\ 1 & 1 & 1 \end{bmatrix}. \quad (\text{A72})$$

We take

$$\mathbf{M} = \begin{bmatrix} V_{11} & V_{21} & V_{31} \\ V_{12} & V_{22} & V_{32} \\ V_{13} & V_{23} & V_{33} \end{bmatrix}, \quad (\text{A73})$$

where the components V_{ij} , $i, j = 1, 2, 3$ are listed in Table IX.

To simplify the expression for V_{11} in Eq. (A72), we begin with the L_{12} term in the denominator

$$\begin{aligned} L_{12} &= z_{11}^2 + 2z_{10}z_{12} + 2z_{11} + 4z_{12} + (1 - p^2) \\ &= F_{11}(p)\left(\frac{\Delta}{\gamma}\right)^2 + F_{12}(p), \end{aligned} \quad (\text{A74})$$

where the terms $F_{11}(p)$, $F_{12}(p)$ are listed in Table VIII.

We find that $F_{11}(p) \gg F_{12}(p)$ for all p and hence

$$L_{12} \approx F_{11}\left(\frac{\Delta}{\gamma}\right)^2. \quad (\text{A75})$$

To further simplify Eq. (A72) we substitute the expressions for a_{10} and a_{12} from Table VI to the expression for V_{11} in Eq. (A72) and use Eq. (A75) to get

$$a_{10} = 1, \quad (\text{A76})$$

$$\begin{aligned} a_{12} &= k_{11} + k_{12} \\ &= -\frac{L_{13}}{L_{12}} - \frac{L_{14}}{L_{12}} + \left(\frac{L_{13}}{L_{12}}\right)^2 \\ &\approx -\frac{L_{14}}{L_{12}} \\ &= -\frac{f_{11}}{(4 + 2z_{10})}\left(\frac{\Delta}{\gamma}\right)^2. \end{aligned} \quad (\text{A77})$$

Using

$$\frac{a_{10} + a_{12}x^2}{L_2} = \frac{1 - \frac{f_{11}}{(4+2z_{10})}\left(\frac{\Delta}{\gamma}\right)^2 \frac{1}{\bar{n}^2}}{F_{11}(p)\left(\frac{\Delta}{\gamma}\right)^2} \quad (\text{A78})$$

we finally obtain a simplified expression for V_{11} ,

$$\begin{aligned} V_{11} &= -p\bar{n}\left(\frac{\Delta}{\gamma}\right)\left[\frac{1 - \frac{f_{11}}{(4+2z_{10})}\left(\frac{\Delta}{\gamma}\right)^2\left(\frac{1}{\bar{n}}\right)^2}{F_{11}(p)\left(\frac{\Delta}{\gamma}\right)^2}\right] \\ &= p\left[-\frac{1}{F_{11}} + \frac{f_{11}}{F_{11}}\frac{1}{(2z_{10} + 4)}\frac{1}{\bar{n}^2}\left(\frac{\Delta}{\gamma}\right)^2\right]\bar{n}\left(\frac{\Delta}{\gamma}\right)^{-1}. \end{aligned} \quad (\text{A79})$$

Proceeding in a similar way we obtain analytic expressions for the other matrix elements V_{ij} listed in Table IX.

Now that we found the analytic expression for the elements of matrix \mathbf{M} , we need to find its inverse:

$$\mathbf{M}^{-1} = \frac{1}{\det(\mathbf{M})}\text{adj}(\mathbf{M}), \quad (\text{A80})$$

where $\det(\mathbf{M})$ is the determinant of \mathbf{M} and $\text{adj}(\mathbf{M})$ is the adjoint of \mathbf{M} .

Using the expressions of V_{ij} in Table IX, we evaluate the minors of \mathbf{M} T_{ij} in order to find its adjoint

$$\begin{aligned} T_{11} &= V_{22}V_{33} - V_{23}V_{32} \\ &= \frac{(3 + z_{20})}{F_{21}}\bar{n}\left(\frac{\Delta}{\gamma}\right)^{-1} - \frac{(3 + z_{30})}{L_{30}}\frac{1}{\bar{n}}\left(\frac{\Delta}{\gamma}\right) \\ &= \left[\frac{(3 + z_{20})}{F_{21}} - \frac{(3 + z_{30})}{F_{31}}\frac{1}{\bar{n}^2}\left(\frac{\Delta}{\gamma}\right)^2\right]\bar{n}\left(\frac{\Delta}{\gamma}\right)^{-1} \\ &= \left[m_1(p) + m_2(p)\frac{1}{\bar{n}^2}\left(\frac{\Delta}{\gamma}\right)^2\right]\bar{n}\left(\frac{\Delta}{\gamma}\right)^{-1}, \end{aligned} \quad (\text{A81})$$

where the coefficients $m_1(p)$, $m_2(p)$ are listed in Table XI.

Proceeding in the same way, we evaluate the remaining minors of \mathbf{M} , i.e., T_{ij} , which are listed in Table X. The coefficients $m_i(p)$ that define T_{ij} are listed in Table XI. All of the coefficients $m_i(p)$ ($i = 1$ to 16) are functions of p only. The adjoint of \mathbf{M} is given by

$$\text{adj}(\mathbf{M}) = \mathbf{M}^T = \begin{bmatrix} T_{11} & T_{12} & T_{13} \\ T_{21} & T_{22} & T_{23} \\ T_{31} & T_{32} & T_{33} \end{bmatrix}, \quad (\text{A82})$$

and the determinant of \mathbf{M} is

$$\det(\mathbf{M}) = V_{11}T_{11} + V_{21}T_{21} + V_{31}T_{31}. \quad (\text{A83})$$

4. Density matrix evolution: Analytical expressions in the overdamped regime $[\Delta/(\bar{n}\gamma) < f(p)]$

In this section we derive analytic expressions for the time evolution of the density matrix. The general solution of the Bloch-Redfield equations [Eq. (3) of the main text] can be obtained from Duhamel's formula (Ref. [22] of the main text)

$$\vec{\mathbf{x}}(t) = e^{A t} \vec{\mathbf{x}}_0 + \int_0^t e^{A(t-s)} \vec{\mathbf{d}} ds, \quad (\text{A84})$$

where

$$\vec{\mathbf{x}}(t) = [\rho_{aa} \quad \rho_{ab}^R \quad \rho_{ab}^I]^T, \quad (\text{A85})$$

$$\vec{\mathbf{x}}_0 = [0 \quad 0 \quad 0]^T \quad (\text{A86})$$

is the initial vector, and

$$\vec{\mathbf{d}} = [r \quad pr \quad 0]^T \quad (\text{A87})$$

is the driving vector. To solve Eq. (A84) we need the exponential of the coefficient matrix \mathbf{A} ,

$$\begin{aligned} e^{t\mathbf{A}} &= \mathbf{M}e^{t\Lambda}\mathbf{M}^{-1} \\ &= \frac{1}{\det(\mathbf{M})} \begin{bmatrix} V_{11} & V_{21} & V_{31} \\ V_{12} & V_{22} & V_{32} \\ V_{13} & V_{23} & V_{33} \end{bmatrix} \begin{bmatrix} e^{\lambda_1 t} & 0 & 0 \\ 0 & e^{\lambda_2 t} & 0 \\ 0 & 0 & e^{\lambda_3 t} \end{bmatrix} \\ &\quad \times \begin{bmatrix} T_{11} & T_{12} & T_{13} \\ T_{21} & T_{22} & T_{23} \\ T_{31} & T_{32} & T_{33} \end{bmatrix} \\ &= \frac{1}{\det(\mathbf{M})} \begin{bmatrix} \phi_{11} & \phi_{21} & \phi_{31} \\ \phi_{12} & \phi_{22} & \phi_{32} \\ \phi_{13} & \phi_{23} & \phi_{33} \end{bmatrix}, \end{aligned} \quad (\text{A88})$$

where \mathbf{M} is the eigenvector matrix found in the previous section, $\Lambda = \begin{bmatrix} \lambda_1 & 0 & 0 \\ 0 & \lambda_2 & 0 \\ 0 & 0 & \lambda_3 \end{bmatrix}$ is the eigenvalue matrix, and

$$\phi_{ij} = \sum_{k=1}^3 e^{\lambda_k t} V_{kj} T_{ki}, \quad i, j = 1-3. \quad (\text{A89})$$

Using Eqs. (A85) to (A88) in Eq. (A84) we get

$$\begin{aligned} \vec{\mathbf{x}}(t) &= \frac{1}{\det(\mathbf{M})} \int_0^t \begin{bmatrix} \phi_{11} & \phi_{21} & \phi_{31} \\ \phi_{12} & \phi_{22} & \phi_{32} \\ \phi_{13} & \phi_{23} & \phi_{33} \end{bmatrix} \begin{bmatrix} r \\ pr \\ 0 \end{bmatrix} ds \\ &= \frac{r}{\det(\mathbf{M})} \int_0^t \begin{bmatrix} \phi_{11} + p\phi_{21} \\ \phi_{12} + p\phi_{22} \\ \phi_{13} + p\phi_{23} \end{bmatrix} ds. \end{aligned} \quad (\text{A90})$$

Evaluating the integrals of $\vec{\mathbf{x}}(t)$ from Eq. (A90), we find the expressions for $\rho_{aa}(t)$, $\rho_{ab}^R(t)$, and $\rho_{ab}^I(t)$,

$$\rho_{aa}(t) = \frac{r}{\det(\mathbf{M})} \sum_{k=1}^3 \frac{(1 - e^{\lambda_k t})}{-\lambda_k} V_{k1}(T_{k1} + pT_{k2}), \quad (\text{A91})$$

$$\rho_{ab}^R(t) = \frac{r}{\det(\mathbf{M})} \sum_{k=1}^3 \frac{(1 - e^{\lambda_k t})}{-\lambda_k} V_{k2}(T_{k1} + pT_{k2}), \quad (\text{A92})$$

$$\rho_{ab}^I(t) = \frac{r}{\det(\mathbf{M})} \sum_{k=1}^3 \frac{(1 - e^{\lambda_k t})}{-\lambda_k} V_{k3}(T_{k1} + pT_{k2}). \quad (\text{A93})$$

To express these general solutions in terms of the physical parameters, we use Eq. (A83) for the determinant of matrix \mathbf{M} and the coefficients V_{ij} , T_{ij} listed in Tables IX and X. The determinant of matrix \mathbf{M} is obtained from Eq. (A83) using

$$\begin{aligned} \det(\mathbf{M}) &= \left\{ p \left[-\frac{m_1}{F_{11}} + \left(-\frac{m_2}{F_{11}} + \frac{f_{11}}{F_{11}} \frac{1}{(2z_{10} + 4)} \right) \frac{1}{\bar{n}^2} \left(\frac{\Delta}{\gamma} \right)^2 \right] + p \left[-\frac{m_5}{F_{21}} - \frac{m_6}{F_{21}} \frac{1}{\bar{n}^2} \left(\frac{\Delta}{\gamma} \right)^2 \right] \right. \\ &\quad \left. + p \left[-\frac{m_{11}}{L_{30}} \frac{1}{\bar{n}^2} \left(\frac{\Delta}{\gamma} \right)^2 - \frac{m_{12}}{L_{30}} \frac{1}{\bar{n}^4} \left(\frac{\Delta}{\gamma} \right)^4 \right] \right\} \bar{n}^2 \left(\frac{\Delta}{\gamma} \right)^{-2}. \end{aligned} \quad (\text{A94})$$

The term proportional to $\frac{1}{\bar{n}^4} \left(\frac{\Delta}{\gamma} \right)^4$ can be neglected for large \bar{n} and we find

$$\begin{aligned} \det(\mathbf{M}) &= p \left[\left(-\frac{m_1}{F_{11}} - \frac{m_5}{F_{21}} \right) + \left(-\frac{m_2}{F_{11}} + \frac{f_{11}}{F_{11}} \frac{1}{(2z_{10} + 4)} - \frac{m_6}{F_{21}} - \frac{m_{11}}{L_{30}} \right) \frac{1}{\bar{n}^2} \left(\frac{\Delta}{\gamma} \right)^2 \right] \bar{n}^2 \left(\frac{\Delta}{\gamma} \right)^{-2} \\ &= \left[T_1(p) + T_2(p) \frac{1}{\bar{n}^2} \left(\frac{\Delta}{\gamma} \right)^2 \right] \bar{n}^2 \left(\frac{\Delta}{\gamma} \right)^{-2}, \end{aligned} \quad (\text{A95})$$

where the coefficients $T_1(p)$, $T_2(p)$ are listed in Table VIII.

To find the expression for $\rho_{aa}(t)$, we calculate the following terms in Eq. (A91):

$$V_{11}(T_{11} + pT_{12}) = \left[A_1 + A_2 \frac{1}{\bar{n}^2} \left(\frac{\Delta}{\gamma} \right)^2 \right] \bar{n}^2 \left(\frac{\Delta}{\gamma} \right)^{-2}, \quad (\text{A96})$$

$$V_{21}(T_{21} + pT_{22}) = \left[A_3 + A_4 \frac{1}{\bar{n}^2} \left(\frac{\Delta}{\gamma} \right)^2 \right] \bar{n}^2 \left(\frac{\Delta}{\gamma} \right)^{-2}, \quad (\text{A97})$$

$$V_{31}(T_{31} + pT_{32}) = \left[A_5 + A_6 \frac{1}{\bar{n}^2} \left(\frac{\Delta}{\gamma} \right)^2 \right], \quad (\text{A98})$$

where the coefficients $A_i(p)$ ($i = 1-6$) are listed in Table XII. All the terms $A_i(p)$ depend on p only. Using Eqs. (96) to (98) in Eq. (91) the general expression of $\rho_{aa}(t)$ can be recast in the form

$$\begin{aligned} \rho_{aa}(t) &= \frac{r}{\det(\mathbf{M})} \left\{ \left[A_1 + A_2 \frac{1}{\bar{n}^2} \left(\frac{\Delta}{\gamma} \right)^2 \right] \bar{n}^2 \left(\frac{\Delta}{\gamma} \right)^{-2} \left(\frac{1 - e^{\lambda_1 t}}{-\lambda_1} \right) \right. \\ &\quad \left. + \left[A_3 + A_4 \frac{1}{\bar{n}^2} \left(\frac{\Delta}{\gamma} \right)^2 \right] \bar{n}^2 \left(\frac{\Delta}{\gamma} \right)^{-2} \left(\frac{1 - e^{\lambda_2 t}}{-\lambda_2} \right) + \left[A_5 + A_6 \frac{1}{\bar{n}^2} \left(\frac{\Delta}{\gamma} \right)^2 \right] \left(\frac{1 - e^{\lambda_3 t}}{-\lambda_3} \right) \right\}. \end{aligned} \quad (\text{A99})$$

Proceeding in the same way as for $\rho_{aa}(t)$, we find the expressions for $\rho_{ab}^R(t)$ and $\rho_{ab}^I(t)$ as

$$\rho_{ab}^R(t) = \frac{r}{\det(\mathbf{M})} \left\{ \left[B_1 + B_2 \frac{1}{\bar{n}^2} \left(\frac{\Delta}{\gamma} \right)^2 \right] \bar{n}^2 \left(\frac{\Delta}{\gamma} \right)^{-2} \left(\frac{1 - e^{\lambda_1 t}}{-\lambda_1} \right) \right. \\ \left. + \left[B_3 + B_4 \frac{1}{\bar{n}^2} \left(\frac{\Delta}{\gamma} \right)^2 \right] \bar{n}^2 \left(\frac{\Delta}{\gamma} \right)^{-2} \left(\frac{1 - e^{\lambda_2 t}}{-\lambda_2} \right) + \left[B_5 + B_6 \frac{1}{\bar{n}^2} \left(\frac{\Delta}{\gamma} \right)^2 \right] \left(\frac{1 - e^{\lambda_3 t}}{-\lambda_3} \right) \right\}, \quad (\text{A100})$$

$$\rho_{ab}^I(t) = \frac{r}{\det(\mathbf{M})} \left\{ \left[C_1 + C_2 \frac{1}{\bar{n}^2} \left(\frac{\Delta}{\gamma} \right)^2 \right] \left(\frac{1 - e^{\lambda_1 t}}{-\lambda_1} \right) \right. \\ \left. + \left[C_3 + C_4 \frac{1}{\bar{n}^2} \left(\frac{\Delta}{\gamma} \right)^2 \right] \left(\frac{1 - e^{\lambda_2 t}}{-\lambda_2} \right) + \left[C_5 + C_6 \frac{1}{\bar{n}^2} \left(\frac{\Delta}{\gamma} \right)^2 \right] \left(\frac{1 - e^{\lambda_3 t}}{-\lambda_3} \right) \right\} \bar{n} \left(\frac{\Delta}{\gamma} \right)^{-1}, \quad (\text{A101})$$

where the coefficients $B_i(p)$, $C_i(p)$ ($i = 1-6$) are listed in Table XII. All the terms $B_i(p)$ and $C_i(p)$ depend on p only.

The general expressions for $\rho_{aa}(t)$, $\rho_{ab}^R(t)$, and $\rho_{ab}^I(t)$ can take two explicit forms depending on the value of the alignment factor p . If the alignment factor is greater than the critical value, i.e., $p > p_c$, then

$$\lambda_j = \gamma z_{j0} \bar{n} = -r |z_{j0}|, \quad j = 1, 3. \quad (\text{A102})$$

However, the second eigenvalue has a different scaling relation as shown in Sec II C of the main text:

$$\lambda_2 = -\gamma |f_{21}| \frac{1}{\bar{n}} \left(\frac{\Delta}{\gamma} \right)^2. \quad (\text{A103})$$

Substituting the eigenvalues from Eqs. (A102) and (A103) into Eqs. (A99) to (A101), using Eq. (A95) for $\det(\mathbf{M})$ and neglecting the small term proportional to $\frac{1}{\bar{n}^4} \left(\frac{\Delta}{\gamma} \right)^4$ for large \bar{n} , we get

$$\rho_{aa}(t) = \frac{1}{[T_1(p) + T_2(p) \frac{1}{\bar{n}^2} \left(\frac{\Delta}{\gamma} \right)^2]} \left\{ \left[A_1 + A_2 \frac{1}{\bar{n}^2} \left(\frac{\Delta}{\gamma} \right)^2 \right] \left(\frac{1 - e^{-\gamma |z_{10}| \bar{n} t}}{|z_{10}|} \right) \right. \\ \left. + \left[A_3 + A_4 \frac{1}{\bar{n}^2} \left(\frac{\Delta}{\gamma} \right)^2 \right] \bar{n}^2 \left(\frac{\Delta}{\gamma} \right)^{-2} \left(\frac{1 - e^{-\gamma |f_{21}| \frac{1}{\bar{n}} \left(\frac{\Delta}{\gamma} \right)^2 t}}{|f_{21}|} \right) + A_5 \frac{1}{\bar{n}^2} \left(\frac{\Delta}{\gamma} \right)^2 \left(\frac{1 - e^{-\gamma |z_{30}| \bar{n} t}}{|z_{30}|} \right) \right\}, \quad (\text{A104})$$

$$\rho_{ab}^R(t) = \frac{1}{[T_1(p) + T_2(p) \frac{1}{\bar{n}^2} \left(\frac{\Delta}{\gamma} \right)^2]} \left\{ \left[B_1 + B_2 \frac{1}{\bar{n}^2} \left(\frac{\Delta}{\gamma} \right)^2 \right] \left(\frac{1 - e^{-\gamma |z_{10}| \bar{n} t}}{|z_{10}|} \right) \right. \\ \left. + \left[B_3 + B_4 \frac{1}{\bar{n}^2} \left(\frac{\Delta}{\gamma} \right)^2 \right] \bar{n}^2 \left(\frac{\Delta}{\gamma} \right)^{-2} \left(\frac{1 - e^{-\gamma |f_{21}| \frac{1}{\bar{n}} \left(\frac{\Delta}{\gamma} \right)^2 t}}{|f_{21}|} \right) + B_5 \frac{1}{\bar{n}^2} \left(\frac{\Delta}{\gamma} \right)^2 \left(\frac{1 - e^{-\gamma |z_{30}| \bar{n} t}}{|z_{30}|} \right) \right\}, \quad (\text{A105})$$

$$\rho_{ab}^I(t) = \frac{1}{[T_1(p) + T_2(p) \frac{1}{\bar{n}^2} \left(\frac{\Delta}{\gamma} \right)^2]} \frac{1}{\bar{n}} \left(\frac{\Delta}{\gamma} \right) \left\{ \left[C_1 + C_2 \frac{1}{\bar{n}^2} \left(\frac{\Delta}{\gamma} \right)^2 \right] \left(\frac{1 - e^{-\gamma |z_{10}| \bar{n} t}}{|z_{10}|} \right) \right. \\ \left. + \left[C_3 + C_4 \frac{1}{\bar{n}^2} \left(\frac{\Delta}{\gamma} \right)^2 \right] \bar{n}^2 \left(\frac{\Delta}{\gamma} \right)^{-2} \left(\frac{1 - e^{-\gamma |f_{21}| \frac{1}{\bar{n}} \left(\frac{\Delta}{\gamma} \right)^2 t}}{|f_{21}|} \right) + \left[C_5 + C_6 \frac{1}{\bar{n}^2} \left(\frac{\Delta}{\gamma} \right)^2 \right] \left(\frac{1 - e^{-\gamma |z_{30}| \bar{n} t}}{|z_{30}|} \right) \right\}. \quad (\text{A106})$$

To further simplify our analytic solutions (A104)–(A106), we note that the coefficients A_i , B_i , and C_i plotted in Fig. 10 do not vary strongly with p in the vicinity of $p = 1$. We can thus replace the coefficients by their limiting values at $p \rightarrow 1$ to yield

$$\rho_{aa}(t) = \frac{1}{[-4 + 1.33 \frac{1}{\bar{n}^2} \left(\frac{\Delta}{\gamma} \right)^2]} \left\{ \left[-4 + 2.92 \frac{1}{\bar{n}^2} \left(\frac{\Delta}{\gamma} \right)^2 \right] \frac{(1 - e^{-4\gamma \bar{n} t})}{4} - \frac{(1 - e^{-0.75 \frac{\gamma}{\bar{n}} \left(\frac{\Delta}{\gamma} \right)^2 t})}{3} + 0.44 \frac{1}{\bar{n}^2} \left(\frac{\Delta}{\gamma} \right)^2 (1 - e^{-\gamma \bar{n} t}) \right\}, \quad (\text{A107})$$

$$\rho_{ab}^R(t) = \frac{1}{[-4 + 1.33 \frac{1}{\bar{n}^2} \left(\frac{\Delta}{\gamma} \right)^2]} \left\{ \left[-4 + 3.249 \frac{1}{\bar{n}^2} \left(\frac{\Delta}{\gamma} \right)^2 \right] \frac{(1 - e^{-4\gamma \bar{n} t})}{4} + (1 - e^{-0.75 \frac{\gamma}{\bar{n}} \left(\frac{\Delta}{\gamma} \right)^2 t}) - 0.89 \frac{1}{\bar{n}^2} \left(\frac{\Delta}{\gamma} \right)^2 (1 - e^{-\gamma \bar{n} t}) \right\}, \quad (\text{A108})$$

$$\rho_{ab}^I(t) = \frac{1}{[-4 + 1.33 \frac{1}{\bar{n}^2} (\frac{\Delta}{\gamma})^2]} \frac{1}{\bar{n}} \left(\frac{\Delta}{\gamma}\right) \left\{ \left[-1.33 + 0.99 \frac{1}{\bar{n}^2} \left(\frac{\Delta}{\gamma}\right)^2 \right] \frac{(1 - e^{-4\gamma\bar{n}t})}{4} - (1 - e^{-0.75 \frac{\Delta}{\bar{n}} (\frac{\Delta}{\gamma})^2 t}) + \left[1.33 - 0.25 \frac{1}{\bar{n}^2} \left(\frac{\Delta}{\gamma}\right)^2 \right] (1 - e^{-\gamma\bar{n}t}) \right\}. \quad (\text{A109})$$

These are Eqs. (27)–(29) of the main text.

If the alignment factor is less than the critical value ($p < p_c$), then

$$\lambda_j = \gamma z_{j0} \bar{n} = -r |z_{j0}|, \quad j = 1, 2, 3. \quad (\text{A110})$$

Substituting the eigenvalues from Eq. (A110) into Eqs. (A99) to (A101), using Eq. (A95) for $\det(\mathbf{M})$ and neglecting the small term proportional to $\frac{1}{\bar{n}^2} (\frac{\Delta}{\gamma})^4$ for large \bar{n} , we get

$$\rho_{aa}(t) = \frac{1}{[T_1(p) + T_2(p) \frac{1}{\bar{n}^2} (\frac{\Delta}{\gamma})^2]} \left\{ \left[A_1 + A_2 \frac{1}{\bar{n}^2} \left(\frac{\Delta}{\gamma}\right)^2 \right] \left(\frac{1 - e^{-\gamma|z_{10}|\bar{n}t}}{|z_{10}|} \right) + \left[A_3 + A_4 \frac{1}{\bar{n}^2} \left(\frac{\Delta}{\gamma}\right)^2 \right] \left(\frac{1 - e^{-\gamma|z_{20}|\bar{n}t}}{|z_{20}|} \right) + A_5 \frac{1}{\bar{n}^2} \left(\frac{\Delta}{\gamma}\right)^2 \left(\frac{1 - e^{-\gamma|z_{30}|\bar{n}t}}{|z_{30}|} \right) \right\}, \quad (\text{A111})$$

$$\rho_{ab}^R(t) = \frac{1}{[T_1(p) + T_2(p) \frac{1}{\bar{n}^2} (\frac{\Delta}{\gamma})^2]} \left\{ \left[B_1 + B_2 \frac{1}{\bar{n}^2} \left(\frac{\Delta}{\gamma}\right)^2 \right] \left(\frac{1 - e^{-\gamma|z_{10}|\bar{n}t}}{|z_{10}|} \right) + \left[B_3 + B_4 \frac{1}{\bar{n}^2} \left(\frac{\Delta}{\gamma}\right)^2 \right] \left(\frac{1 - e^{-\gamma|z_{20}|\bar{n}t}}{|z_{20}|} \right) + B_5 \frac{1}{\bar{n}^2} \left(\frac{\Delta}{\gamma}\right)^2 \left(\frac{1 - e^{-\gamma|z_{30}|\bar{n}t}}{|z_{30}|} \right) \right\}, \quad (\text{A112})$$

$$\rho_{ab}^I(t) = \frac{1}{[T_1(p) + T_2(p) \frac{1}{\bar{n}^2} (\frac{\Delta}{\gamma})^2]} \frac{1}{\bar{n}} \left(\frac{\Delta}{\gamma}\right) \left\{ \left[C_1 + C_2 \frac{1}{\bar{n}^2} \left(\frac{\Delta}{\gamma}\right)^2 \right] \left(\frac{1 - e^{-\gamma|z_{10}|\bar{n}t}}{|z_{10}|} \right) + \left[C_3 + C_4 \frac{1}{\bar{n}^2} \left(\frac{\Delta}{\gamma}\right)^2 \right] \left(\frac{1 - e^{-\gamma|z_{20}|\bar{n}t}}{|z_{20}|} \right) + \left[C_5 + C_6 \frac{1}{\bar{n}^2} \left(\frac{\Delta}{\gamma}\right)^2 \right] \left(\frac{1 - e^{-\gamma|z_{30}|\bar{n}t}}{|z_{30}|} \right) \right\}. \quad (\text{A113})$$

Equations (A111)–(A113) are identical to Eqs. (30)–(32) of the main text.

In the limit of small energy level spacing ($\frac{\Delta}{\gamma} \ll 1$) and large \bar{n} , we can neglect the terms proportional to $\frac{1}{\bar{n}^2} (\frac{\Delta}{\gamma})^{-2}$ in the above equations and the general solution further simplifies. For $p > p_c$, we obtain

$$\rho_{aa}(t) = \frac{1}{T_1(p)} \left[A_1 \left(\frac{1 - e^{-\gamma|z_{10}|\bar{n}t}}{|z_{10}|} \right) + A_4 \left(\frac{1 - e^{-\gamma|f_{21}| \frac{1}{\bar{n}} (\frac{\Delta}{\gamma})^2 t}}{|f_{21}|} \right) \right], \quad (\text{A114})$$

$$\rho_{ab}^R(t) = \frac{1}{T_1(p)} \left[B_1 \left(\frac{1 - e^{-\gamma|z_{10}|\bar{n}t}}{|z_{10}|} \right) + B_4 \left(\frac{1 - e^{-\gamma|f_{21}| \frac{1}{\bar{n}} (\frac{\Delta}{\gamma})^2 t}}{|f_{21}|} \right) \right], \quad (\text{A115})$$

$$\rho_{ab}^I(t) = \frac{1}{T_1(p)} \left(\frac{\Delta}{\bar{n}\gamma}\right) \left[C_1 \left(\frac{1 - e^{-\gamma|z_{10}|\bar{n}t}}{|z_{10}|} \right) + C_4 \left(\frac{1 - e^{-\gamma|f_{21}| \frac{1}{\bar{n}} (\frac{\Delta}{\gamma})^2 t}}{|f_{21}|} \right) + C_5 \left(\frac{1 - e^{-\gamma|z_{30}|\bar{n}t}}{|z_{30}|} \right) \right]. \quad (\text{A116})$$

Equations (A114)–(A116) are the same as Eqs. (33)–(35) of the main text.

For $p < p_c$ we find

$$\rho_{aa}(t) = \frac{1}{T_1(p)} \left[A_1 \left(\frac{1 - e^{-\gamma|z_{10}|\bar{n}t}}{|z_{10}|} \right) + A_3 \left(\frac{1 - e^{-\gamma|z_{20}|\bar{n}t}}{|z_{20}|} \right) \right], \quad (\text{A117})$$

$$\rho_{ab}^R(t) = \frac{1}{T_1(p)} \left[B_1 \left(\frac{1 - e^{-\gamma|z_{10}|\bar{n}t}}{|z_{10}|} \right) + B_3 \left(\frac{1 - e^{-\gamma|z_{20}|\bar{n}t}}{|z_{20}|} \right) \right], \quad (\text{A118})$$

$$\rho_{ab}^I(t) = \frac{1}{T_1(p)} \left(\frac{\Delta}{\bar{n}\gamma}\right) \left[C_1 \left(\frac{1 - e^{-\gamma|z_{10}|\bar{n}t}}{|z_{10}|} \right) + C_3 \left(\frac{1 - e^{-\gamma|z_{20}|\bar{n}t}}{|z_{20}|} \right) + C_5 \left(\frac{1 - e^{-\gamma|z_{30}|\bar{n}t}}{|z_{30}|} \right) \right]. \quad (\text{A119})$$

The above equations are the same as Eqs. (36)–(38) of the main text.

- [1] M. Schlosshauer, *Decoherence and The Quantum-to-Classical Transition* (Springer, Berlin, 1997).
- [2] H.-P. Breuer and F. Petruccione, *The Theory of Open Quantum Systems* (Clarendon, Oxford, 2006), Chap. 3.4.
- [3] M. O. Scully and M. S. Zubairy, *Quantum Optics* (Cambridge University Press, Cambridge, UK, 1997).
- [4] C. L. Degen, F. Reinhard, and P. Cappellaro, Quantum sensing, *Rev. Mod. Phys.* **89**, 035002 (2017).
- [5] T. D. Ladd, F. Jelezko, R. Laflamme, Y. Nakamura, C. Monroe, and J. L. O'Brien, Quantum computers, *Nature (London)* **464**, 45 (2010).
- [6] M. Fleischhauer, C. H. Keitel, M. O. Scully, and C. Su, Lasing without inversion and enhancement of the index of refraction via interference of incoherent pump processes, *Opt. Commun.* **87**, 109 (1992).
- [7] G. C. Hegerfeldt and M. B. Plenio, Coherence with incoherent light: A new type of quantum beats for a single atom, *Phys. Rev. A* **47**, 2186 (1993).
- [8] G. S. Agarwal and S. Menon, Quantum interferences and the question of thermodynamic equilibrium, *Phys. Rev. A* **63**, 023818 (2001).
- [9] V. V. Kozlov, Y. Rostovtsev, and M. O. Scully, Inducing quantum coherence via decays and incoherent pumping with application to population trapping, lasing without inversion, and quenching of spontaneous emission, *Phys. Rev. A* **74**, 063829 (2006).
- [10] B.-Q. Ou, L.-M. Liang, and C.-Z. Li, Coherence induced by incoherent pumping field and decay process in three-level Λ -type atomic system, *Opt. Commun.* **281**, 4940 (2008).
- [11] M. O. Scully, K. R. Chapin, K. E. Dorfman, M. B. Kim, and A. Svidzinsky, Quantum heat engine power can be increased by noise-induced coherence, *Proc. Natl. Acad. Sci. USA* **108**, 15097 (2011).
- [12] K. E. Dorfman, D. V. Voronine, S. Mukamel, and M. O. Scully, Photosynthetic reaction center as a quantum heat engine, *Proc. Natl. Acad. Sci. USA* **110**, 2746 (2013).
- [13] T. V. Tscherbul and P. Brumer, Long-lived Quasistationary Coherences in a V -type System Driven by Incoherent Light, *Phys. Rev. Lett.* **113**, 113601 (2014).
- [14] A. Dodin, T. V. Tscherbul, and P. Brumer, Quantum dynamics of incoherently driven V -type systems: Analytic solutions beyond the secular approximation, *J. Chem. Phys.* **144**, 244108 (2016).
- [15] A. Dodin, T. V. Tscherbul, and P. Brumer, Coherent dynamics of V -type systems driven by time-dependent incoherent radiation, *J. Chem. Phys.* **145**, 244313 (2016).
- [16] M. Macovei, J. Evers, and C. H. Keitel, Quantum correlations of an atomic ensemble via an incoherent bath, *Phys. Rev. A* **72**, 063809 (2005).
- [17] G. S. Agarwal, *Quantum Statistical Theories of Spontaneous Emission and their Relation to Other Approaches* (Springer, Berlin, 1974).
- [18] K. P. Heeg *et al.*, Vacuum-Assisted Generation and Control of Atomic Coherences at X-Ray Energies, *Phys. Rev. Lett.* **111**, 073601 (2013).
- [19] K. Blum, *Density Matrix Theory and Applications* (Springer, Berlin, 2011).
- [20] C. Creatore, M. A. Parker, S. Emmott, and A. W. Chin, Efficient Biologically Inspired Photocell Enhanced by Delocalized Quantum States, *Phys. Rev. Lett.* **111**, 253601 (2013).
- [21] A. Fruchtmann, R. Gómez-Bombarelli, B. W. Lovett, and E. M. Gauger, Photocell Optimization Using Dark State Protection, *Phys. Rev. Lett.* **117**, 203603 (2016).
- [22] W. E. Boyce and R. C. DiPrima, *Elementary Differential Equations* (Wiley, New York, 2008).
- [23] Z. Ficek and S. Swain, *Quantum Interference and Coherence* (Springer, New York, 2005), pp. 57–58.
- [24] M. Kiffner, M. Macovei, J. Evers, and C. H. Keitel, Vacuum-induced processes in multilevel atoms, *Prog. Opt.* **55**, 85 (2010).
- [25] M. Fleischhauer, A. Imamoglu, and J. P. Marangos, Electromagnetically induced transparency: Optics in coherent media, *Rev. Mod. Phys.* **77**, 633 (2005).
- [26] A. Dodin, T. V. Tscherbul, R. Alicki, A. Vutha, and P. Brumer, Non-secular Redfield dynamics and Fano coherences in incoherent excitation: An experimental proposal, *Phys. Rev. A* **97**, 013421 (2018).
- [27] T. F. Gallagher, *Rydberg Atoms* (Cambridge University Press, Cambridge, UK, 1994).
- [28] T. V. Tscherbul and P. Brumer, Coherent dynamics of Rydberg atoms in cosmic-microwave-background radiation, *Phys. Rev. A* **89**, 013423 (2014).
- [29] V. N. Shatokhin, M. Walschaers, F. Schlawin, and A. Buchleitner, Coherence turned on by incoherent light, [arXiv:1602.07878](https://arxiv.org/abs/1602.07878).
- [30] B. Çakmak, A. Manatuly, and Ö. E. Möstecaplıoğlu, Thermal production, protection, and heat exchange of quantum coherences, *Phys. Rev. A* **96**, 032117 (2017).